CHALMERS
UNIVERSITY OF TECHNOLOGY

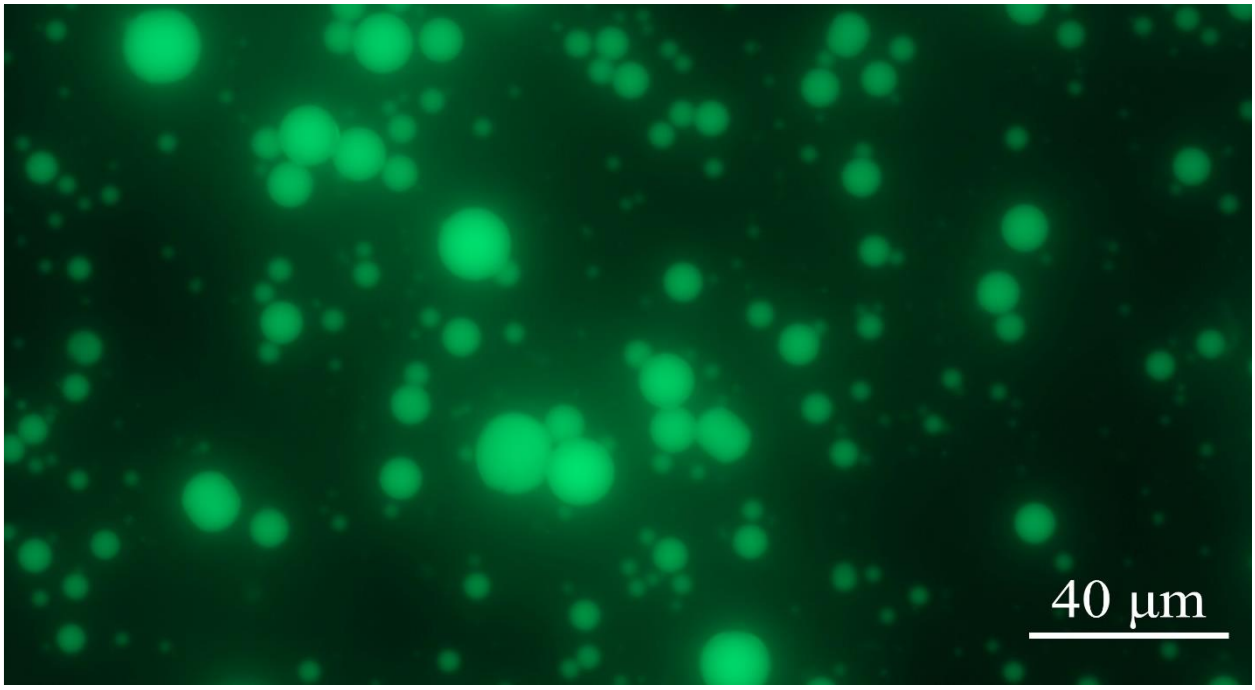

Tuning the molecular diffusion in microcapsules for a sustained release of antifoulants

Master's thesis in Materials Chemistry

SOFIA EDEGRAN

DEPARTMENT OF CHEMISTRY AND CHEMICAL ENGINEERING
CHALMERS UNIVERSITY OF TECHNOLOGY
Gothenburg, Sweden 2022
www.chalmers.se

MASTER'S THESIS 2022

Tuning the molecular diffusion in microcapsules for a sustained release of antifoulants

SOFIA EDEGRAN

CHALMERS
UNIVERSITY OF TECHNOLOGY

Department of Chemistry and Chemical Engineering
Division of Applied Chemistry
CHALMERS UNIVERSITY OF TECHNOLOGY
Gothenburg, Sweden 2022

Tuning the molecular diffusion in microcapsules for a sustained release of antifoulants
SOFIA EDEGRAN

Supervisors: Lars Evenäs, Chalmers University of Technology
Viktor Eriksson, Chalmers University of Technology
Markus Andersson Trojer, RISE Research Institutes of Sweden

Examiner: Lars Evenäs, Chalmers University of Technology

Master's Thesis 2022
Department of Chemistry and Chemical Engineering
Division of Applied Chemistry
Chalmers University of Technology
SE-412 96 Gothenburg
Telephone +46 31 772 1000

Cover: Fluorescence microscopy image of polylactic acid microspheres.

Gothenburg, Sweden 2022

Tuning the molecular diffusion in microcapsules for a sustained release of antifoulants
SOFIA EDEGRAN
Department of Chemistry and Chemical Engineering
Chalmers University of Technology

Abstract

Marine biofouling is a serious economic and environmental concern as fouling organisms on ship hulls cause pollution by increasing the friction drag and forcing a higher fuel consumption. Fouling can be avoided temporarily by dispersing biocides in marine paints. A long-term protection, however, is difficult to achieve as the small molecular size of the biocides renders a fast diffusional leakage through the coating matrix. A promising approach to sustain the release, and thus prolonging its functional lifetime, is microencapsulation of the biocides.

In this project the biocidal compound tralopyril has been encapsulated into polymeric microcapsules through a solvent evaporation method. Several microcapsule systems have been assessed by their loading capacities and release characteristics, through a screening based on morphology and capsule constituents. The material selection was limited to biodegradable capsule constituents to be applicable in a real marine environment. Further, the most promising capsules have been incorporated in a marine paint system, where their performance has been evaluated relative to commercial paint formulations with freely dispersed biocide.

It was found that a core-shell morphology was not suited for encapsulation of tralopyril, due to a disadvantageous solubility preference. Encapsulation in monolithic microspheres was therefore superior and could be optimized by selecting a polymer with a suitable chemical composition and molecular weight. Lactic-based polymers performed significantly better than polyhydroxybutyrate, with pure polylactic acid (PLA) being superior in terms of encapsulation efficiency and lower diffusivity. Increasing the molecular weight led to a more sustained release, but potentially also a lower loading capacity.

Incorporation of PLA spheres in a marine paint was successful from a formulation and release perspective. Coatings containing encapsulated biocide had a significantly more sustained release compared to coatings with freely dispersed biocide. Thus, by tuning the molecular diffusion in microcapsules an overall sustained release from antifouling coatings can be achieved.

Keywords: biocide leakage, microcapsule, microsphere, solvent evaporation, diffusion, controlled release, tralopyril, PLA, PLGA, PHB

Acknowledgements

I would like to thank my supervisors, Lars Evenäs, Markus Andersson Trojer and Viktor Eriksson for their support throughout this project. I feel so lucky to work with such great people. Lars, thank you for always having my back. You give great advice and I learn so much from you. Markus, you have been a huge help in keeping the project move forward. Thank you for all your ideas and enthusiasm. Viktor, thank you for taking care of me and teaching me everything I know about laboratory work. You are so skilled, and I look up to you so much.

I would also like to thank everyone who has contributed to this master's thesis. Alexander Idström, thank you for interpreting my NMR spectra. Fredrik Edhborg, thank you for teaching me how to do fluorescence spectroscopy. Fanny Bjarnemark, thank you for conducting the LC-MS analyses. To all members of the research groups of Lars Evenäs and Romain Bordes, thank you for your valuable inputs during our group meetings.

Lastly, I would like to thank family and friends. A special thanks to Fredrik, you make me so happy!

Sofia Edegran, Gothenburg, June 2022

Contents

List of figures

List of tables

1
Introduction

Marine biofouling, the accumulation of living organisms on subaqueous surfaces, is an extensive problem. As of today, more than 4000 fouling species have been identified, ranging from bacteria and microalgae to seaweeds and barnacles. Fouling affects ships, bridges and subsea equipment, such as aquaculture cages, sonar devices and underwater cables (1,2). The direct consequences of fouling, as well as the conventional countermeasures to combat it, have considerable adverse economic and environmental effects. First, biofouling causes increased pollution and green-house gas emissions. The growth of fouling organisms on ship hulls leads to increased friction drag and hence a loss in speed, higher fuel consumption and engine stress. A direct consequence of the higher fuel consumption is increased pollution. A 5% increase in biofouling leads to a 17% higher fuel consumption and a 14% increase in greenhouse gas emissions (3). Furthermore, fouling contributes to the spread of invasive species. Naval traffic transports fouling organisms to new habitats, which in the long run can cause a reduction in biodiversity and damage to resource sectors such as fisheries and aquaculture. There is also an associated risk of spreading diseases carried by the fouling organisms (2). Lastly, other problems arising from fouling include increased loadings which can sink buoys and damage fishing nets. Acid-producing bacteria in biofilms can induce and sustain corrosion in marine environments. There are also safety concerns regarding biofouling as wet algae are slippery (3).

Historically, the prevention of biofouling has always been achieved by surface coatings. Records date back to ancient civilizations where coatings of pitch, wax, tar or asphaltite were used as protection (4,5). Later, the Romans began to clad their wooden ships with lead and copper (6) and this strategy remained in use for centuries. It was eventually phased out in the 19th century because modern steel ships suffered from galvanic corrosion when coated with a more noble metal. Instead, a new and fast-growing market of antifouling paints emerged (5), already in 1865 there were 300 patents issued in England (6). The paints constituted, and still do today, of polymeric matrices with dispersed antifouling biocides. Tributyltin, introduced in the 1960s, was the first widely successful biocide due to its broad-spectrum toxicity against many fouling species (5). However, after its usage peaked at the end of the 20th century, severe ecotoxicological effects became evident and the substance was banned globally in 2008 (7). Protection is nowadays achieved through a cocktail of complementary and less hazardous biocides (8,9). The biocide substance tralopyril, for instance, is especially efficient against shell-building marine organisms (10).

Contemporary coatings are associated with a major problem though; a too fast and premature biocidal leakage. This is detrimental for the long-term antifouling performance of the coating, and indirectly also causing biocidal pollution. For efficient protection, the concentration of biocide on the coating surface must exceed a minimum inhibitory concentration (MIC) that is maintained by a continuous and sustained diffusional migration through the matrix (8). The apparent diffusion is dependent both on the size of the diffusing species, as well as the pore structure of the dry-film coating. It may therefore differ vastly depending on the paint system (9). Still, as most organic biocides are small molecules with a high inherent diffusivity, the leakage through the paint matrix will be both excessive and rapid, leading to concentrations far above the MIC. Exposure levels below the MIC of any remaining biocide content can in turn cause microbial resistance (11). One way to prolong the antifouling effect of the coating is to compensate for the early leakage by adding high amounts of biocides to the paint formulation. However, the slight gain in antifouling durability should be carefully weighed against the negative aspects of this approach; it is expensive, it might impair the thermo-mechanical properties of the coating, and it is causing unnecessary biocidal pollution (8,9). A better solution is to instead control the biocidal release through microencapsulation. This way, concentrations far above the MIC can be avoided – eliminating the excessive pollution – while at the same time extending the functional lifetime of the coating. Microcapsules offer a versatile way to tune the diffusion-dependent release through a number of parameters; including the size and size distribution of the capsules, the morphology, and the chemical nature of the capsule materials (12).

1.1 Purpose and objectives

The purpose of the project is to sustain the biocidal release rate from antifouling coatings through microencapsulation. Different microcapsule formulations will be screened and evaluated based on the capsules loading capacities and release characteristics. A sufficient loading capacity for the biocide is important, so that the capsule materials added to the paint formulation are of such a low amount so that other properties of the paint such as film formation, wettability, or opacity remain unaffected. Regarding the release characteristics, it is desired that the biocide concentration at the coating surface is kept just above the MIC for a prolonged period. This can be tuned if the apparent diffusion coefficient for a capsule formulation is known.

A first objective of the project is to screen different capsule formulations based on morphologies and capsule constituents. Polymeric materials will be evaluated on the effects of chemical composition, molecular weight, degree of crystallinity and type of end-group. A second objective is to incorporate the microcapsules in a marine paint system. The release of molecularly free biocide will be compared to the release of encapsulated biocide.

1.2 Limitations

Limitations applies to both the material choice, as well as the experimental methodology used in this project. In order to be incorporated in a marine paint system the capsules need to be biodegradable, which limits the selection of capsule constituents. Also, the biocide encapsulated in this project has been limited to tralopyril. Tralopyril can biodegrade through hydrolysis and is therefore promising in an environmental perspective (7).

Regarding the methodology it will be limited to an experimental protocol utilized by the research group (9,13). Microcapsules are formulated through a coacervation method, internal phase separation by solvent evaporation, and subsequently characterized by optical microscopy. Release studies, for the microcapsule suspensions and the antifouling coatings, respectively, are performed in aqueous media. At certain time points measurements are taken and the released biocide is quantified with a suitable analytical technique. The effect of molecularly free biocide versus encapsulated biocide in antifouling coatings will only be evaluated based on the biocidal release to artificial seawater. Due to the limited timeframe of the project, the antifouling efficacy in a real marine environment will not be measured.

2
Theory

2.1 Microcapsules

Microcapsules are colloidal particles whose main functions are to protect and control the release of active substances: biocides, preservatives or pharmaceuticals, et cetera. The umbrella term “microcapsule” includes a multitude of morphologies, with the simplest being the microsphere, illustrated in Figure 2.1a. Microspheres consist of a monolithic, often polymeric, matrix in which the active substance is homogeneously distributed. Among the more complex two-phase morphologies, the most useful for controlled release is the core-shell particle (Figure 2.1b). Here, a solid shell covers a core material in which the active substance is dissolved. Different core materials range from hydrophobic oils to aqueous media. Other two-phase morphologies also exist, such as the acorn particle (Figure 2.1c) with a partially encapsulated core (12,13).

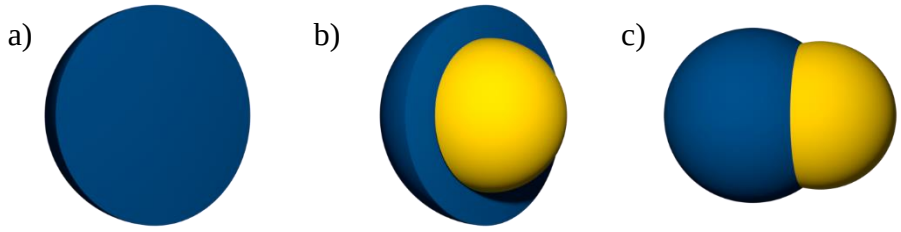

Figure 2.1 Three different microcapsule morphologies, a) microsphere, b) core-shell particle and c) acorn particle.

2.2 Internal phase separation by solvent evaporation

Microencapsulation can be achieved through a variety of methods. Polymerization methods such as emulsion polymerization and interfacial polycondensation rely on chemical reactions. There are also physical or mechanical means to produce the microcapsules. These include spray-drying, Layer-by-Layer assembly and solvent evaporation, among others (12,14). Internal phase separation by solvent evaporation is a coacervation method first described by Loxley and Vincent in 1998 (15). It has gained popularity for many reasons; (i) it does not leave any residues, such as monomers, (ii) the microcapsule dimensions are easily controlled, and (iii) it is straightforward and suitable for industrial scale-up (8). In principle, this method produces microcapsules from an oil-in-water emulsion by controlled phase separation within the emulsion droplets. The constituents of the desired microcapsules, that is the polymeric shell material, the core oil and the active substance, are dissolved in a volatile solvent. The one-phase system is then added to an aqueous solution under high-shear mixing to form the

oil-in-water emulsion. Once the emulsion is formed, the volatile solvent is let to evaporate, which causes the remaining constituents in the dispersed phase to phase separate and organize into microcapsules. The final morphology can be predicted through thermodynamic considerations which will be discussed in more detail later.

The starting components need to fulfil several requirements for successful encapsulation. A limited, but sufficient, water solubility of the volatile solvent is needed for evaporation to take place while maintaining the integrity of emulsion droplets. The volatile solvent should be chosen so that the constituents of the microcapsules are able to completely dissolve. Furthermore, the polymer and the core oil must be water-insoluble, and the core oil should be a nonsolvent for the polymer. Finally, the core oil and the polymer should be chosen so that the active substance preferentially dissolves in the core oil. The procedure for making microspheres is identical except that no core material is added.

2.2.1 Predicting the microcapsule morphology

For thermodynamical equilibrium, the final microcapsule morphology should correspond to the minimization of the total free energy in the system. This can be calculated (15) from the interfacial tensions, γ_{ij}, between the core oil (o), the polymeric shell (p) and the aqueous phase (w) respectively. For each phase a spreading coefficient, S_i, is determined according to,

$$S_i = \gamma_{jk} - (\gamma_{ij} + \gamma_{ik}). \tag{2.1}$$

The final morphology is then predicted through the four possible combinations of the spreading coefficients,

$$S_o < 0; \quad S_w < 0; \quad S_p > 0, \tag{2.2}$$

$$S_o < 0; \quad S_w < 0; \quad S_p < 0, \tag{2.3}$$

$$S_o < 0; \quad S_w > 0; \quad S_p < 0, \tag{2.4}$$

$$S_o > 0; \quad S_w < 0; \quad S_p < 0. \tag{2.5}$$

The spreading conditions in Equation 2.2 predict core-shell particles, while Equation 2.3 favors the formation of acorn particles, both of which are illustrated in Figure 2.1. When Equation 2.4 is fulfilled separate droplets of the polymeric shell and the core oil are formed. Satisfaction of Equation 2.5 is rare, but would result in inverted core-shell particles, where the core oil encapsulates the polymeric shell material.

2.3 Microcapsule size distribution

As most emulsions follow a log-normal size distribution (16), it is reasonable to assume that this also applies to microcapsules prepared via the solvent evaporation method. The log-normal distribution of the capsule radius, r, is presented in Equation 2.6. Here, μ and σ are the mean and standard deviation of $\ln(r)$. The mean, μ_r, and standard deviation, σ_r, of r can be determined through Equations 2.7 and 2.8.

$$p(r) = \frac{1}{r\sigma\sqrt{2\pi}} \exp\ (-\frac{(\ln r - \mu)^2}{2\sigma^2}) \tag{2.6}$$

$$\mu_r = \exp\ (\mu + \frac{\sigma^2}{2}) \tag{2.7}$$

$$\sigma_r^2 = \exp\ (2\mu + \sigma^2)(\exp(\sigma^2) - 1) \tag{2.8}$$

2.4 Microcapsule constituents

The microcapsule constituents are chosen based on three criteria. First, the core oil and the shell polymer should favor the formation of core-shell particles. For the oil to remain inside a surrounding polymer shell the spreading conditions in Equation 2.2 must be satisfied. Capsule compositions that fulfill these conditions have previously been investigated by the research group (17). Second, both the core oil and the polymer need to be biodegradable to be applied in a marine paint system, in order to avoid microplastic pollution and to comply with the most recent and impending European regulations. Third, the core material must be able to dissolve the active substance.

Accounting for the three criteria, two oils, glyceryl trioctanoate and ethyl linoleate, were found suitable. Glyceryl trioctanoate, Figure 2.2, is a relatively short chained triglyceride. Triglycerides are the main constituent of plant and animal fat (18). Ethyl linoleate, Figure 2.3, is the fatty acid ester of ethanol and linoleic acid (19). It occurs in nature as a plant metabolite (20).

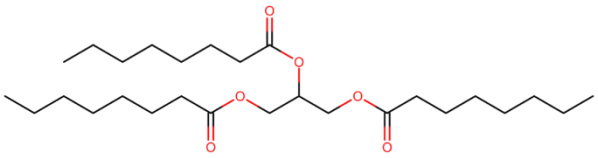

Figure 2.2 Molecular structure of glyceryl trioctanoate.

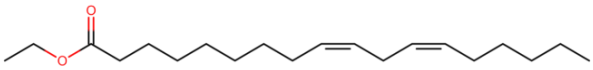

Figure 2.3 Molecular structure of ethyl linoleate.

2.4.1 Polymers

To meet the requirement of biodegradability, the polymer selection has been limited to aliphatic polyesters, which can hydrolyze in water. The choice of polymer is important as it affects the loading capacity, stability and sustained release properties of the microcapsules. To optimize the encapsulation, different aliphatic polyesters have hence been screened based on: chemical composition, molecular weight, degree of crystallinity and type of end-group of the polymer. The molecular weight influences the polymer packing and the porosity of the microparticle (21). The permeability of the active substance through the capsule matrix is also affected by the degree of crystallinity (22,23). The end-group has only a slight effect on the overall chemical nature of the polymer but can still contribute significantly to the effective diffusion of the active substance. For example, if a chemical interaction between the end-group and the active exists (24). The polymer types tested in this work are presented below.

2.4.1.1 Polylactic acid

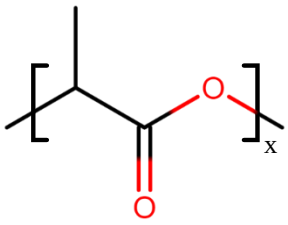

Figure 2.4 Molecular structure of polylactic acid.

Polylactic acid (PLA), Figure 2.4, is an aliphatic polyester which is both biobased and biodegradable, thus becoming increasingly important in today's transition towards a circular economy. PLA can be synthesized from lactic acid or lactide, which are produced in fermented sugars. Lactic acid (LA) is a chiral molecule with two optically active configurations, the L-isomer and the D-isomer. In nature the L-isomer is much more abundant, facilitating the production of pure poly-L-lactic acid (PLLA) (25,26). The relative content of the two enantiomers has a strong impact on the physical properties of the polymer. PLA grades consisting of more than 93% of L-LA are semi-crystalline, while grades with lower optical purity are amorphous (26,27). Pure PLLA has a glass transition temperature of 63°C, which decreases with increasing D-isomer content (26).

2.4.1.2 Poly(lactic-co-glycolic acid)

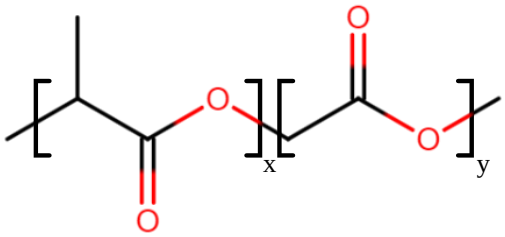

Figure 2.5 Molecular structure of poly(lactic-co-glycolic acid).

Similar to PLA is poly(lactic-co-glycolic acid) (PLGA), the copolymer of LA and glycolic acid (GA). The structural formula can be seen in Figure 2.5. Even though the homopolymers of pure LA or GA may be semicrystalline, the copolymer is always amorphous (28,29). PLGA is synthesized either directly from its monomeric acids, or through ring-opening polymerization of lactide and glycolide (28). Structurally the comonomers only differ in the presence of a methyl side group on LA, which is absent on GA. Yet, the comonomer ratio largely affects the physical properties of PLGA. A higher content in LA results in a more hydrophobic polymer, less prone to water absorption and hence with a lower rate of the hydrolysis reaction (29,30). Degradation times can differ from a few weeks to several months, but is generally slower the higher the content in LA (29). Moreover, the glass transition temperature is also affected by the comonomer ratio. It is usually close to 50 °C and increases with the LA content (28).

2.4.1.3 Polyhydroxybutyrate

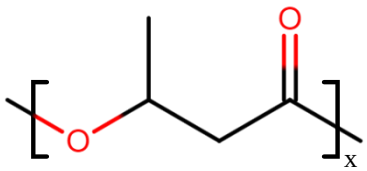

Figure 2.6 Molecular structure of poly(3-hydroxybutyrate).

Another biobased and biodegradable polymer is polyhydroxybutyrate (PHB), which is a member of the class of aliphatic polyesters called polyhydroxyalkanoates (PHA). These polymers are produced by prokaryotic microorganisms under an excess of carbon sources and a limited supply of other nutrients. In nature, PHAs function as carbon and energy storage materials, even though the main interest from an industrial perspective lies in their unique mechanical properties. Their discovery date back to the 1920s when poly(3-hydroxybutyrate) (P3(HB)), see Figure 2.6, was isolated from bacteria (31–34).

PHB has an exceptional stereoregularity and is almost completely isotactic. The degree of crystallinity is therefore very high, ranging from 50 to 80% (31–33). PHB is a stiff and brittle material, with excellent barrier properties provided by the structure of the crystalline lamellae (31,32). The glass transition temperature for P3(HB) is approximately 5 °C (31).

2.5 Active substance

The usage of biocides is strictly regulated within the European Union (35). Substances are continuously evaluated and banned based on bioaccumulation and environmental persistence or toxicity. Marketed today as more eco-friendly alternatives to their predecessors is a new generation of biocides (7). This new generation includes the substance denoted tralopyril, shown in Figure 2.7.

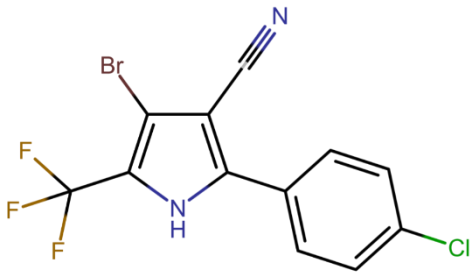

Figure 2.7 Molecular structure of tralopyril.

Tralopyril is produced by Janssen Pharmaceuticals and sold under the trademark Econea®. Tralopyril has a high antifouling efficacy towards shell-building marine organisms, but is less efficient towards algae (10). The substance inhibits cellular energy production by uncoupling the oxidative phosphorylation in mitochondria (36,37). Ultimately, this may impair the nervous system of fouling organisms (37). When released into water most tralopyril is converted within one day to its hydrolysis product. That is a structurally similar compound, with the only difference being the exchange of the trifluoromethyl for a carboxyl group. The hydrolysis product is not readily biodegradable (7).

2.6 Marine paints

Paints can be used for aesthetic and protective purposes, or as a means of surface modification. For marine paints, which spend most of their service life underwater, the antifouling and anticorrosive properties of the coating are of the highest importance (38).

Paint constituents can be divided into four categories: solvent, binder, pigments and additives. Depending on the type of solvent, paints are classified as solvent-based or waterborne. In a solvent-based paint, the binder material is molecularly dissolved in an organic solvent, such as an aliphatic hydrocarbon or alcohol, whereas in a waterborne paint the binder is instead dispersed in an aqueous phase. The solvent facilitates the coating application and is then evaporated, so it is not present in a dry-film coating. The continuous phase of the dry coating matrix is provided by the binder. The binder is usually a film-binding polymeric material, which can carry and bind the particulate components in the paint together. Pigments give the paint its color, while additives are used to enhance the chemical

and physical properties of both the in-can paint and the dry coating (38,39). For antifouling paints, biocides are essential additives.

In contemporary marine paints, the biocides are molecularly dispersed (8), and the leakage through the dry-film coating is governed by the effective diffusivity inside the polymeric matrix. It is important to be aware that this is influenced by the pore structure of the coating. The porosity can vary substantially between different paint systems and is also highly affected by the conditions during the drying of the coated film (9).

2.7 Diffusion models

Biocidal release is governed by diffusion, that is the random movement of the antifouling compounds inside a matrix, and it can therefore be modelled through general diffusion equations. The diffusional concentration gradient as a function of time is expressed through Fick's second law of diffusion (40), which in its simplest form concerns one-dimensional motion in isotropic media,

$$\frac{\partial C}{\partial t} = D\frac{\partial^2 C}{\partial x^2}. \tag{2.9}$$

Here, C is the concentration of the diffusing substance, D is the diffusion coefficient, t is the time and x is the space coordinate. Often, it is advantageous to model the fractional release, $m(t)/m_{tot}$, rather than the concentration.

2.7.1 Diffusion in a sphere

Diffusion-dependent release from microspheres follows Crank's solution (40) to Equation 2.9 for a spherical geometry,

$$f_s(r,t) = \frac{\alpha_s}{1+\alpha_s}\left[1 - \sum_{n=1}^{\infty} \frac{6\alpha_s(\alpha_s+1)}{9+9\alpha_s+q_{s,n}^2\alpha_s^2} \exp\left(-\frac{Dq_{s,n}^2 t}{r^2}\right)\right]. \tag{2.10}$$

As should be noted, the fractional release, f_s, is a function of the sphere radius, r, and the time, t. The parameter α_s is the equilibrium mass distribution of active substance between the release medium and the microspheres, and can be calculated from,

$$\alpha_s = \frac{V_{sink}}{V_{sphere}K}. \tag{2.11}$$

Here, K is the partition coefficient, V_{sink} the total volume of the release medium and V_{sphere} the total volume of the suspended microspheres. The parameter $q_{s,n}$ is the n:th positive root of

$$\tan q_{s,n} = \frac{3q_{s,n}}{3+\alpha_s q_{s,n}^2}. \tag{2.12}$$

However, Equation 2.10 is valid for microspheres of a single radius, r, and does not take the polydispersity into account. The complete expression for the fractional release is therefore weighted according to the volume distribution, recall the log-normal radius distribution, $p(r)$, presented in Equation 2.6.

$$\frac{m(t)}{m_{\text{tot}}} = \frac{\int f_s(r,t)p(r)r^3 \mathrm{d}r}{\int p(r)r^3 \mathrm{d}r} \tag{2.13}$$

2.7.2 Diffusion in a plane sheet

Similar to the release from microspheres, the diffusional leakage from a coating matrix can be derived from Fick's second law. Assuming perfect sink conditions, that is a maximum biocide concentration orders of magnitude below the saturation concentration, the partition coefficient *K* can be neglected. This simplifies Crank's solution (40) for diffusion in a plane sheet and the fractional release, f_c, can be expressed through Equation 2.14. Note that the thickness of the sheet is given by *L*.

$$f_c(L,t) = 1 - \sum_{n=0}^{\infty} \frac{8}{(2n+1)^2\pi^2} \exp\left(-\frac{D(2n+1)^2\pi^2 t}{4L^2}\right) \tag{2.14}$$

2.8 Characterization techniques

Characterization techniques have been used for determination of chemical and physical properties (spectroscopic techniques), sample visualization and localization of the active (microscopic techniques), as well as quantification of the active (spectrometric techniques).

2.8.1 Nuclear magnetic resonance spectroscopy

Nuclear magnetic resonance (NMR) spectroscopy is based on the magnetic properties of atoms. Nuclei have angular momentum and thus generate a magnetic field. The nuclear magnetic moment is quantized and therefore there exists a discrete and finite number of energy levels, so-called spin states, which a nucleus can occupy. In an NMR spectrometer the spins align parallel to a strong external magnetic field. Not all nuclei will have spins in the lowest energy state, the ground state, but there will be a Boltzmann distribution according to Equation 2.15,

$$\frac{N_x}{N_0} = \exp\left(\frac{-\Delta E}{kT}\right), \tag{2.15}$$

where *N* is the number of nuclei in an excited state *x* respectively the ground state 0. ΔE is the energy difference between the states, k is the Boltzmann constant and *T* is the absolute temperature. The hydrogen atom (^{1}H) has two spin states (41).

By irradiating with electromagnetic radiation, the intrinsic spin property of atomic nuclei can become excited to higher energy states. The resonance frequencies for these transitions are recorded by the NMR spectrometer and give information about the chemical environment of the excited nuclei. In a ^{1}H NMR spectrum additional important information is stored as well. Splitting of resonance peaks occurs due to spin-spin coupling, that is magnetic interactions between different nuclei. Also, the area under the resonance peak is proportional to the number of protons that contribute to that signal. For these reasons a ^{1}H NMR spectrum can be used to determine the chemical structure of an unknown protonated compound (41).

2.8.2 Ultraviolet-visible spectrophotometry

Ultraviolet-visible (UV-Vis) absorption spectrophotometry focuses on excitations of electrons instead of nuclear spins, which is achieved by electromagnetic radiation of higher energy. According to the Beer-Lambert law, Equation 2.16, the absorption is linearly dependent on the concentration of the analyte molecule,

$$A = \log_{10}\left(\frac{I_0}{I}\right) = \varepsilon(\lambda)cl. \tag{2.16}$$

A is the absorption, I_0 and I is the intensity before and after passing through the sample. ε is the molar absorptivity, which is dependent on the wavelength λ, c is the concentration of the analyte and l is the path length the light passes through the sample (42).

2.8.3 Fluorescence spectroscopy and microscopy

Fluorescence techniques are based on deexcitations of electrons. There are multiple pathways for relaxation back into the ground state for a molecule that has become excited to a higher electronic state. The energy can be dissipated as heat through collisions between molecules in solution or through fluorescence by emission of a photon. The fraction of the absorbed photons that is emitted as fluorescence is expressed through the fluorescence quantum yield, Φ. This can be determined through relative actinometry (43),

$$\Phi = \Phi_r \frac{A_r}{A}\frac{E}{E_r}\frac{\eta^2}{\eta_r^2}, \tag{2.17}$$

where the subscript r denotes a reference compound of known fluorescence quantum yield, A is the absorption at the excitation wavelength, E is the integrated emission intensity and η is the refractive index.

A spectrofluorometer is generally able to record two types of spectra, both the excitation of and emission from a fluorophore. An emission spectrum is obtained by exciting the compound at a single excitation wavelength, and then measuring the emission at a range of wavelengths. Conversely, an excitation spectrum focuses on the emission intensity at a certain wavelength by scanning the excitation wavelength. For most fluorophores, the shape of the excitation spectrum mimics the absorption spectrum (43).

When working with fluorescent molecules there are several important characteristics to be aware of. First, there are several vibrational states associated with each electronic state. An excited molecule generally decays to the lowest associated vibrational state before relaxing back to its electronic ground state, this energy loss is the reason why emission is of higher wavelengths than absorption. Second, because of the immediate decay to the lowest vibrational state the emission spectrum is independent of the excitation wavelength, which is known as Kasha's rule. Third, for many molecules the spacing of the vibrational energy levels in the excited states are almost identical to those in the ground state. This causes the emission spectrum to be the mirror image of the absorption spectrum, resulting from the ground to first excited state transition (43), as seen in Figure 2.8.

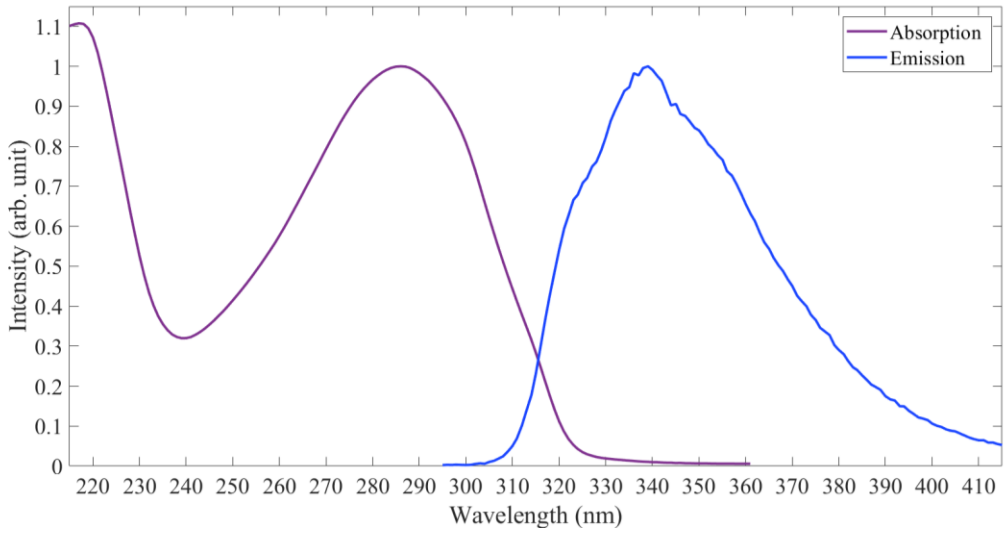

Figure 2.8 The absorption and emission spectra of tralopyril. Note that the emission spectrum is the mirror image of the absorption peak at 286 nm.

2.8.4 Liquid chromatography-mass spectrometry

Liquid chromatography-mass spectrometry (LC-MS) is a combined technique for separation, identification and quantification of analytes. Chromatography, as a collective term, concerns separation of mixtures based on relative partitioning of analytes between different phases. A mobile phase is carried past a stationary phase, where analytes are retained and separated depending on their respective affinities for each phase. A higher affinity for the stationary phase directly correlates with a longer retention time (44). MS is a sensitive and highly specific analytical technique for identification and quantification. Analytes are ionized and distinguished based on their respective mass-to-charge (*m*/*z*) ratio (44,45).

In high-performance liquid chromatography (HPLC) the mobile phase is pressurized, as it passes through closed columns containing the stationary phase, to increase the chromatographic resolution. The best performing instruments employ ultrahigh-pressure and are trademarked as UPLC by Waters Corporation. Different modes of operation are possible, for example either normal-phase or reversed-phase chromatography. In normal-phase chromatography the stationary phase is more polar than the mobile phase, whereas the opposite is true for reversed-phase chromatography. Another option to consider is whether to elute under isocratic or gradient conditions. Isocratic elution means that the mobile phase composition remains constant during the separation procedure, whereas in a gradient elution the mobile phase composition gradually changes to decrease the retention of late-eluting components (44).

While HPLC operates under high pressure, MS requires high vacuum to prevent ions from colliding during the mass-to-charge separation (44). For the devices to be compatible, an LC-MS setup therefore needs a suitable interface between. A mass spectrometer consists of three main components: an ionization source, a mass analyzer and a detector. Ideally the ionization source can also serve as the interface, which is a reason why electrospray ionization (ESI) is a popular method of choice. In ESI, ions are generated at atmospheric pressure by the application of high voltage to the HPLC eluate to create a charged aerosol. The ions subsequently vaporize from the aerosol and enter the mass analyzer. In the mass

analyzer ions are sorted by their *m*/*z* ratios, through external electric or magnetic fields (44,45). Analyses of complex mixtures can be achieved through multiple connected mass analyzers, so-called MS/MS. An example is the common mass analyzer: the quadrupole, which series-coupled becomes the triple quadrupole (QqQ) instrument (45). Finally, the ion current reaches the detector, where the abundances of each species are determined (44).

3
Methods

3.1 Materials

All chemicals, acetone (≥ 99.8%, VWR Chemicals), acetone-d6 (99.9 atom% D, Sigma-Aldrich), acetonitrile (99.8%, Sigma-Aldrich), chloroform (≥ 99.5%, Sigma-Aldrich), dichloromethane (Sigma-Aldrich), 2,5-diphenyloxazole (99%, Sigma-Aldrich), ethanol (99.5% Analytical Grade, Solveco), ethyl acetate (≥ 99.5%, Sigma-Aldrich), ethyl linoleate (≥ 99%, Sigma-Aldrich), formic acid (≥ 99%, Sigma-Aldrich), glyceryl trioctanoate (≥ 99%, Sigma-Aldrich), methanol (≥ 99.9% , Sigma-Aldrich), phosphoric acid (85%, Honeywell Fluka™), poly(3-hydroxybutyric acid) (M_n 10,000, Sigma-Aldrich), polyoxyethylene(23)monododecyl ether (Brij® L23, Sigma–Aldrich), poly(lactic-co-glycolic acid) (65:35, M_w 40,000-75,000, Sigma-Aldrich), poly(lactic-co-glycolic acid) (70:30, M_w 10,000, Polysciences, Inc.), poly(lactic-co-glycolic acid) (M_w 7,000-17,000, Resomer® RG 502, Sigma-Aldrich), poly(lactic-co-glycolic acid) (M_w 7,000-17,000, Resomer® RG 502 H, Sigma-Aldrich), poly(lactic-co-glycolic acid) (M_w 38,000-54,000, Resomer® RG 504 H, Sigma-Aldrich), poly-D,L-lactic acid (M_w 15,000, Polysciences, Inc.), poly-L-lactic acid (IV 0.8-1.2 dL/g, Resomer® L 206 S, Sigma-Aldrich), poly(vinyl alcohol) (95% hydrolysed, M_w 95,000, Acros Organics), and tralopyril (Econea®, Janssen PMP) were used as received.

A commercially available and biocide-free marine paint was provided by Steen-Hansen. Artificial seawater was prepared by mixing simulated sea salt (Lake Products Company LLC), according to the standard ASTM D1141-98, with the appropriate amount of distilled water. Except for the artificial seawater, the water used throughout the project was of Milli-Q purity (resistivity 18.2 MΩ cm, Millipore).

3.2 Characterization of the active

When encapsulating an active it is important to be aware of its purity so that no contaminants interfere with the detection and analytical quantification of the substance. The optical properties are highly important since UV-Vis spectrophotometry is a convenient method for quantification. Moreover, the location of an encapsulated fluorescent molecule can be visualized in a microscope.

UV-Vis absorption spectra were recorded on a Cary 50 spectrophotometer (Varian, USA). The fluorescence properties were investigated on a Cary Eclipse Fluorescence Spectrophotometer (Varian, USA), both excitation spectra and emission spectra at different wavelengths were obtained. The solvent for tralopyril was either ethanol or an aqueous

solution of 0.5 wt% non-ionic surfactant Brij® L23. The quantum yield for tralopyril, at excitation wavelength 290 nm, was determined relative to a reference, 2,5-diphenyloxazole in methanol ($\Phi_r = 0.71$).

Purification of the active was achieved by solid-liquid extraction. To extract any impurities the biocide powder was dispersed in dichloromethane, which is a non-solvent for tralopyril, and the sample was centrifuged on a BR4i centrifuge (Jouan, France). An orange supernatant, containing some pigmented impurity, was removed from the white tralopyril pellet. The purified tralopyril was further analyzed with fluorescence spectroscopy.

Moreover, after evaporating the dichloromethane and drying the extracted impurity, ^{1}H NMR spectroscopy was used for structural identification and quantification of the impurity. The contaminant, purified tralopyril and non-purified tralopyril, respectively, were dissolved in acetone-d6 and analyzed on a Varian 400 MHz spectrometer (Varian, USA).

3.3 Microcapsule formulation

Emulsification was achieved by a Polytron PT 3100 D with PT-DA 07/2EC-F101 as dispersing aggregate (Kinematica, Switzerland). A 5 mL round bottom flask with a side neck (Ace glass, USA) was used. Half of the water phase (1 wt% poly(vinyl alcohol)) was added immediately to the round bottom flask, for the microspheres and core-shell particles that is 2.5 mL respectively 3 mL. A homogenizing speed of 4000 rpm was applied. An oil phase was prepared according to Table 3.1, and then added slowly to the water phase. Emulsification was carried out for 60 minutes. Thereafter the emulsion was diluted with the remainder of the water phase and left in a fume hood overnight under gentle magnetic stirring, while the volatile solvent evaporated. The final microcapsule concentration in suspension was approximately 2 wt%.

Table 3.1 Composition of the oil phase before evaporation, for microspheres and core-shell particles, respectively. The amount of active substance, expressed as a weight percentage of the total mass of shell material and core oil, was varied in different microcapsule formulations.

Morphology	Active (wt%)	Shell material (g)	Core oil (g)	Chloroform (g)
Microsphere	5-10	0.1000	—	2.67
Core-shell	1-6	0.1000	0.0330	3.20

3.4 Microscopy analysis

To visualize the microcapsules an Axio Imager Z2m microscope (Zeiss, Germany) equipped with an HBO-lamp and bandpass filter sets 38HE, 43 and 49 for fluorescence imaging was used. Techniques applied were brightfield and differential interference contrast (DIC), to determine surface structure and morphology. Brightfield micrographs were also used to obtain microcapsule size distributions. At least 500 particles per batch, for almost all batches, were counted and analyzed with the image-processing software ImageJ (National Institute of Health, USA). Moreover, other utilized microscopy techniques were polarized light, to detect crystalline materials in the capsule suspension, and fluorescence, to see the location of the active substance in the capsules.

3.5 Paint formulation and coating application

Two different paint formulations were to be evaluated, either with molecularly free biocide or encapsulated biocide. The amount of biocide in the wet paint was kept constant at 0.30 wt%, regardless of the system. For the paint with freely dispersed biocide, tralopyril dissolved in a small amount of ethyl acetate was added to and thoroughly mixed with the paint formulation. For the paint with encapsulated tralopyril, PLA microspheres loaded with 10 wt% tralopyril were prepared. The reason for the chosen capsule formulation was promising results, in terms of loading capacity and release rate, in the earlier microsphere studies.

Prior to adding the spheres to the paint, the water content in the sphere suspension had to be reduced. This was achieved by a stepwise centrifugation, from 30xg to 1500xg, on a BR4i centrifuge (Jouan, France), to target microspheres of different sizes. After each step, the sediment was collected, and the supernatant transferred to a new centrifuge tube for repeated centrifugation. The sediment was then added to the paint, which after mixing was immediately coated onto substrates to prevent early biocidal leakage from the spheres to the wet formulation.

The substrates used were polypropylene plates, conditioned on one side using P180 sandpaper (Sia Abrasives, Switzerland) in order to ensure full adhesion of the dry film to the surface. A 100 µm thick layer at a 5 x 5 cm area, carefully measured and taped around the edges, was coated on each plate using a Bird Film Applicator (Elcometer, UK) mounted to an automatic film applicator (TQC, The Netherlands). The traverse speed was set to 20 mm/s. After the wet coating application the plates were left to dry in a fume hood for seven days. A picture of a coated plate can be seen in Figure 3.1.

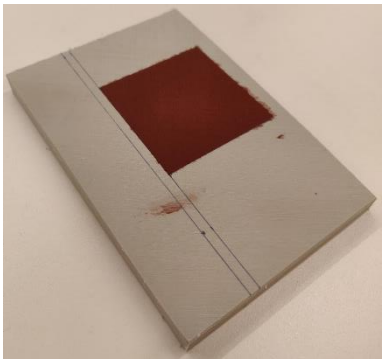

Figure 3.1 A polypropylene substrate coated at a 5 x 5 cm area.

A total of 10 plates were coated; four plates with molecularly free biocide, four plates with encapsulated biocide and two biocide-free plates as a reference. Each plate was weighted before and after the wet coating application, as well as after drying. The dry-film coating thickness was measured for one plate using an Alpha-Step D-100 profilometer (KLA-Tencor, USA).

3.6 Release measurements

A release study follows the amount of leached biocide as a function of time. The biocide-loaded material, in this project either a microcapsule suspension or a coating, is put in a stirred release medium. At certain time points aliquots are taken and the amount of released substance is quantified with a suitable analytical technique.

3.6.1 Release from microcapsules

For microcapsules, the release medium was an aqueous solution of 0.5 wt% Brij® L23. The reason for having the non-ionic surfactant in the release medium was to increase the saturation concentration of the biocide, which enabled a more accurate estimate of the

diffusion coefficient from the measured data. The biocide diffusivity inside the capsules remained unaffected. Release baths were each in total 40 mL, containing approximately 250 mg/L suspended microparticles. This particle concentration was chosen so that the biocidal leakage could be quantified within the linear range of the analytical instrument, a UV-Vis spectrophotometer (Agilent 8453, USA).

At certain time points aliquots of 1.5 mL were taken from the release bath for quantification. Immediately after a sample was taken the suspended microcapsules had to be removed to prevent further leaching of biocide. For the first aliquot this was done by filtering through a 13 mm syringe filter with a 0.2 µm PTFE membrane (Fisher Scientific, USA), as it was desirable to get an as early measurement as possible. The following aliquots were separated by centrifugation, 17000xg for 2 minutes, on a VWR Micro Star 17 centrifuge (Avantor, USA).

To determine the total concentration of biocide in the release bath an aliquot of 0.5 mL was taken and diluted with 1.5 mL ethanol. The sample was left overnight under gentle shaking before centrifugation and analysis. Since ethanol is a good solvent for the biocide this procedure ensured that all had been extracted from the capsules.

After centrifugation the samples were transferred to quartz cuvettes and their concentrations were determined, at the maximum absorbance wavelength for tralopyril at 286 nm, by UV-Vis spectrophotometry.

3.6.2 Release from coatings

Recall from Section 3.5 that a total of 10 plates were coated; four with paint containing molecularly free biocide, four with paint containing encapsulated biocide and two with biocide-free paint. One plate of each kind was saved for determination of the respective total biocide content, while the rest were used to study the biocidal release.

To imitate the real environment for the marine coatings, artificial seawater was chosen as release medium. Release baths were each in total 3 L, thus achieving sink conditions with a release medium volume 50 times greater than the volume of a saturated solution. Coated plates were positioned 45° tilted face-down in the release baths and put on a mechanical shaker for a gentle stirring. An image of the setup is shown in Figure 3.2. Apart from the coated plates, also a bath containing solely artificial seawater was studied, in order to detect any introduction of potential contaminants as the measurements progressed.

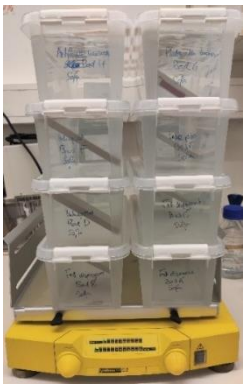

Figure 3.2 Gently shaken release baths.

A low concentration of the biocide required a sensitive analytical technique for quantification, which is why LC-MS/MS was chosen. The procedure for collecting samples was adapted accordingly. At given times, duplicate 4 mL samples were taken from each release bath. Tralopyril was stabilized by the addition of 4 µL 85% phosphoric acid and the samples were stored in the freezer until the analysis. Out of the two samples from the bath containing solely artificial seawater, one was left completely blank for potential contaminant quantification. The other artificial seawater sample was spiked with 10 µL 4 mg/L tralopyril in acetonitrile/0.1% formic acid, as a way to follow the hydrolysis of tralopyril during storage. Samples that had been stored for an equal amount of time were assumed to have degraded proportionally to the reference sample. After samples had been collected, the release baths were refilled with 8 mL artificial seawater each.

Prior to analysis, samples were prepared by centrifugation to remove any interfering fall-off materials from the coatings. The samples were centrifuged for 10 minutes each, either on a 5430R centrifuge (Eppendorf, Germany) at 7200xg, or on a VWR Mega Star 1.6R (Avantor) at max speed 10300 rpm. The samples were then diluted and the content of tralopyril and its hydrolysis product were quantified by LC-MS/MS (Acquity UPLC i-class/ Xevo TQ-XS, Waters, USA). Chromatographic separation was achieved with a 2 min linear gradient from mobile phase A (95:5 water: acetonitrile/0.1% formic acid) to mobile phase B (acetonitrile/0.1% formic acid), over a reversed-phase C18 column (Acquity UPLC CSH C18, 130 Å ,1.7 µm, 2.1 mm × 50 mm, Waters, USA). The QqQ mass spectrometer was run with ESI in negative mode.

4
Results and discussion

4.1 Properties of the active

The fluorescence quantum yield for tralopyril, at excitation wavelength 290 nm, was determined to be 2.0%. The molecule hence only displayed a very faint fluorescence.

The emission from tralopyril was studied at different excitation wavelengths. Tralopyril have absorption and emission maxima at 286 nm and 340 nm (Figure 2.8), respectively. A contaminant was discovered when the non-purified sample was excited at 365 nm, which had distinctly different absorption and emission characteristics compared to the biocide. The characteristics of the contaminant are shown in Figure 4.1 (solid lines). As should also be noted, purification of the active was achieved successfully. After extraction with dichloromethane, the substance emitting at 400-500 nm was almost completely removed, see Figure 4.1 (dashed lines). The emission spectrum of tralopyril was unaffected by the purification process.

What was positive was that the absorption of the contaminant did not interfere with the absorption of the active. This made UV-Vis spectrophotometry a feasible method for quantification of the biocide.

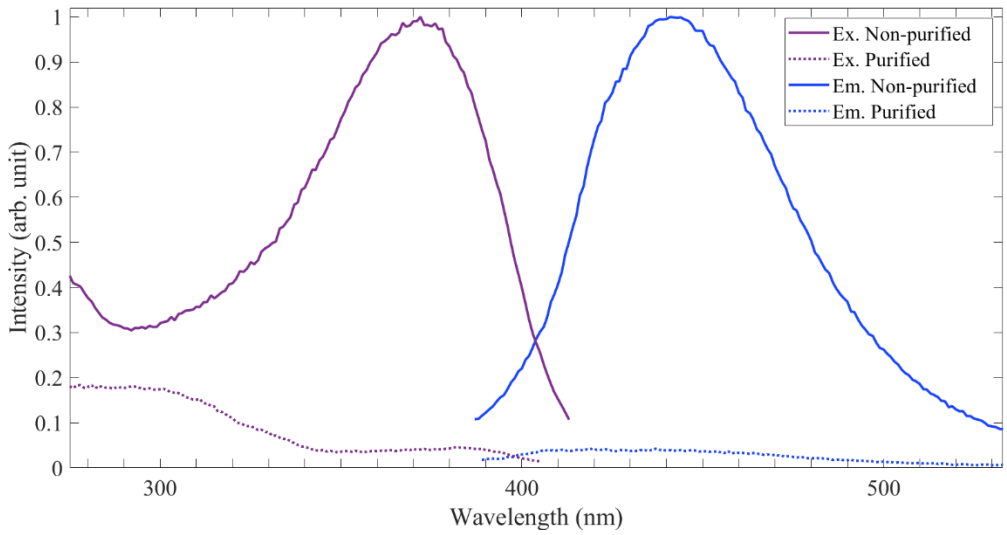

Figure 4.1 Excitation (Ex., purple) and emission (Em., blue) spectra, for a non-purified (solid lines) versus a purified (dashed lines) sample of the tralopyril grade from Janssen PMP. The excitation wavelength, for the emission spectrum, is 365 nm, and the emission wavelength, for the excitation spectrum is 440 nm. The excitation and emission spectra of the non-purified sample are distinctly different from the characteristics of pure tralopyril, hence indicating the presence of a contaminant.

The ^{1}H NMR analyses confirmed the presence of approximately 1 mol% contaminant in the technical grade of tralopyril. While it was difficult to do a complete structural determination, due to interfering signals of tralopyril in the sample containing up-concentrated contaminant, a few functional groups could still be identified. Similar to tralopyril, the contaminant contained an aromatic structure. Unlike tralopyril, the contaminant possessed an ethyl group, and possibly also an aldehyde group.

4.2 Core-shell particles

Core-shell particles were screened based on (i) biocide loading, either 1 or 6 wt% tralopyril, (ii) core oil, glyceryl trioctanoate or ethyl linoleate were used, and (iii) polymeric shell material. Two different low molecular weight (~10,000 Da) PLGA grades, differentiated by the comonomer ratios, were used. A more hydrophobic grade with a 70:30 lactic to glycolic ratio, and a 50:50 grade, respectively.

All formulations yielded a core-shell morphology with a slightly offset core regardless of the capsule constituents. For a representative image see Figure 4.2. Changing the PLGA grade made no discernible difference on the microparticles, but by varying the core oil an interesting fluorescence phenomenon was discovered. For the fluorescence microscopy analysis different bandpass filters were used, those limits both the excitation and emission wavelengths to narrow ranges in order to block out interfering signals and study only a selected fluorescence from the sample. When ethyl linoleate was used as core oil, the fluorescence intensity was higher in the shell compared to the core in all studied bandpass filters (blue, green and red). However, when glyceryl trioctanoate was used as core oil (Figure 4.3) the fluorescence intensity was higher in the core relative to the shell in the blue bandpass filter, whereas the opposite was true in the green and red bandpass filter, respectively. A higher fluorescence intensity directly correlates with a higher concentration of fluorescent molecules.

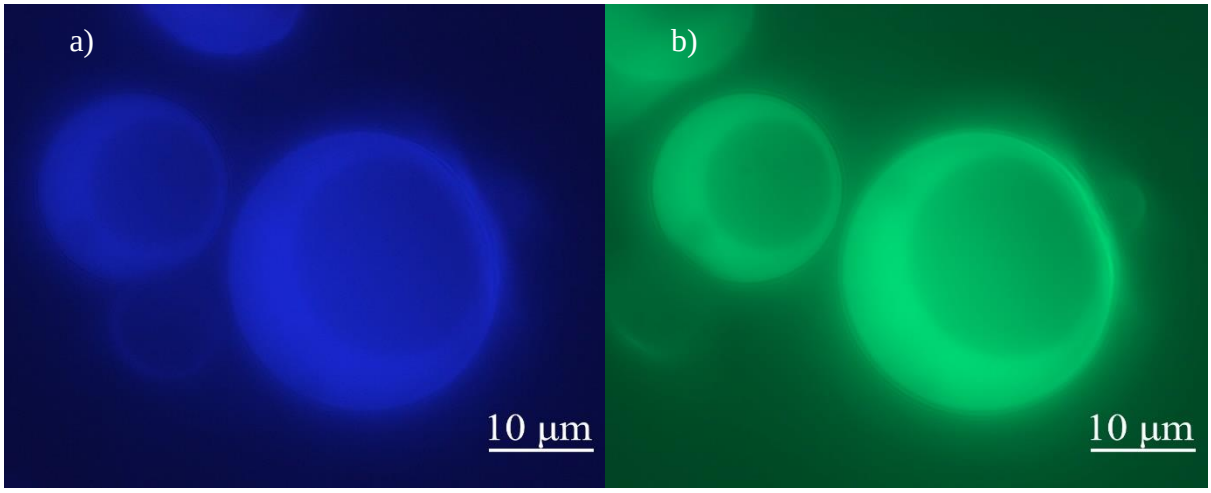

Figure 4.2 Core-shell particles of PLGA 70:30 and ethyl linoleate. Visualized by fluorescence microscopy with a) a blue bandpass filter and b) a green bandpass filter.

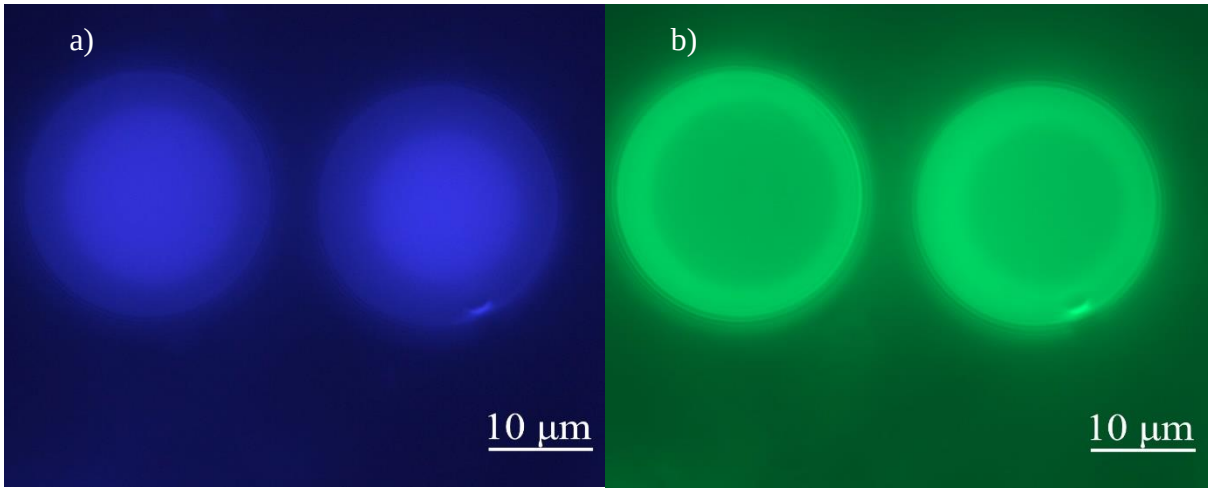

Figure 4.3 Core-shell particles of PLGA 50:50 and glyceryl trioctanoate. Visualized by fluorescence microscopy with a) a blue bandpass filter and b) a green bandpass filter.

The apparent contradiction between the different bandpass filters could be explained by the contaminant present in the technical grade of tralopyril. The excitation (300-400 nm) and emission (420-470 nm) range of the blue bandpass filter coincided well with the excitation and emission spectra of the contaminant (Figure 4.1). Recall that the fluorescence quantum yield for tralopyril was only 2.0%, meaning that 1 mol% of highly fluorescent contaminant could dominate the emission output recorded by the microscope. By changing the core oil, the partitioning of the contaminant was shifted from the shell towards the core.

The excitation wavelengths for the green and red bandpass filters were higher (>450 nm) and so the emission recorded here was not attributed to the contaminant. Instead, it was deemed more likely that it was the faint tail of tralopyril's absorption curve (stretching above 600 nm) that was causing the fluorescence. Since the fluorescence intensity was higher in the shell compared to the core in the green and red bandpass filters for all capsule formulations, an unfortunate preferential solubility of the biocide in the polymer was concluded. This morphology is hence not the best suited for encapsulation of tralopyril.

Regarding the biocide loading, 1 wt% tralopyril was able to completely dissolve in the core-shell particles, whereas formulations containing 6 wt% resulted in large amounts of crystallized tralopyril in suspension. This indicated saturated microcapsules, and for determination of the capsule loading capacity the biocidal release was studied for one batch.

4.2.1 Release study of a core-shell particle suspension

In Figure 4.4 the release profile for a core-shell particle batch of PLGA 50:50 and glyceryl trioctanoate, loaded with 6 wt% tralopyril, is shown. Note the logarithmic x-axis and that the release is expressed as a fraction of the total concentration of biocide. The sharp increase in biocide concentration during the first hour was to a large extent caused by dissolution of crystalline tralopyril in suspension, recall that formulations containing 6 wt% resulted in saturated core-shell particles. Accounting for the crystalline fraction (~0.7) of the total amount of biocide, the loading capacity of the core-shell particles was estimated to be less than 2 wt%. After the crystalline dissolution, the release was purely diffusion-dependent, as the remaining biocide content had been successfully encapsulated.

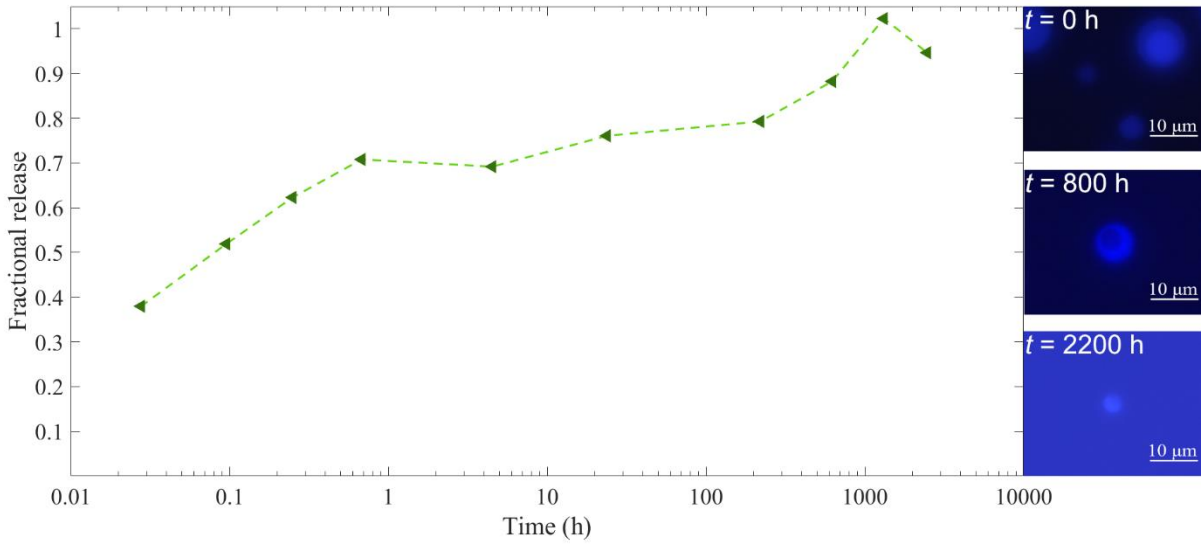

Figure 4.4 Left, fractional release of tralopyril from core shell particles (PLGA 50:50, glyceryl trioctanoate, 6 wt% tralopyril), note the logarithmic x-axis. Right, the diffusional leakage of the contaminant, present in the technical grade of tralopyril, visualized with fluorescence microscopy. The migration from the core to the surrounding aqueous medium could be followed as the measurement progressed.

The insets to the right in Figure 4.4 show the diffusional leakage of the contaminant, present in the technical grade of tralopyril, visualized with fluorescence microscopy. As the measurement progressed the contaminant migrated from the core (0 h) via the shell (800 h), to the surrounding aqueous medium (2200 h). The corresponding fluorescence micrographs for tralopyril, obtained with the usage of a green bandpass filter, are similar, except tralopyril was already located in the capsule shell at the beginning of the measurement.

4.3 Microspheres

Monolithic microspheres were screened based on (i) chemical composition, different aliphatic polyesters were tested, (ii) molecular weight, either a low molecular weight (~10,000 Da) or a higher (>40,000 Da), (iii) degree of crystallinity, ranging from completely amorphous to semi-crystalline polymers, and (iv) type of end-group, where some grades had been modified and end-capped with an alkyl ester instead of the original carboxylic acid. An overview is shown in Table 4.1. The biocide loading was held constant at 10 wt% tralopyril, except for one batch of PLGA 70:30 spheres loaded with 5 wt%.

Table 4.1 Overview of the different polymers used for microsphere formulations.

Label	Polymer	Comonomer ratio (LA:GA)	M_w (kDa)	Crystallinity	End-group
A	PLGA	50:50	~10	Amorphous	Ester
B	PLGA	50:50	~10	Amorphous	Acid
C	PLGA	50:50	>40	Amorphous	Acid
D	PLGA	65:35	>40	Amorphous	Acid
E	PLGA	70:30	~10	Amorphous	Acid
F	PLA	-	~10	Amorphous	Acid
G	PLLA	-	>40	Semi-crystalline	Ester
H	P3(HB)	-	~10	Semi-crystalline	Acid

4.3.1 Microscopy characterization

In general, microspheres formulated with a low molecular weight grade of lactic-based polymers (PLA and PLGA) yielded the most promising results in terms of capsule morphology and homogeneity. The capsules were stable and had a uniform spherical geometry. A representative image is shown in Figure 4.5.

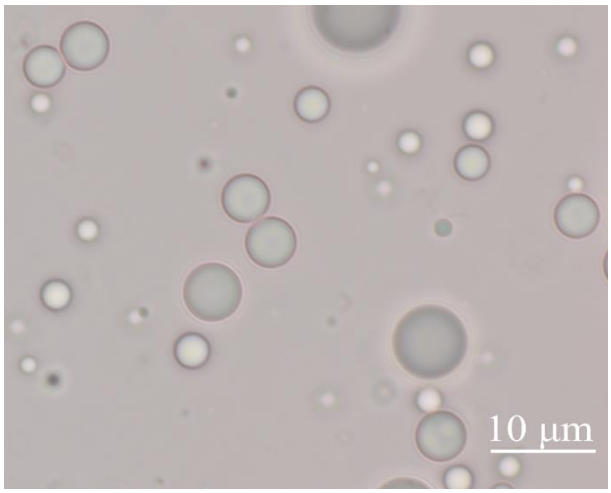

Figure 4.5 PLA microspheres visualized by brightfield microscopy.

Microspheres formulated with a higher molecular weight grade of PLGA surprisingly obtained a core-shell structure, where droplets of the surrounding aqueous phase likely had been encapsulated within the polymeric microparticles. Typical surface structures can be seen in Figure 4.6a, note that some spheres had a singular core, some multiple cores and some were homogenous without any core. In fluorescence microscopy analyses (Figure 4.6b) a lower fluorescence intensity in the cores compared to the shell were observed, which could be attributed to tralopyril's low water solubility and confirmed that the cores were aqueous.

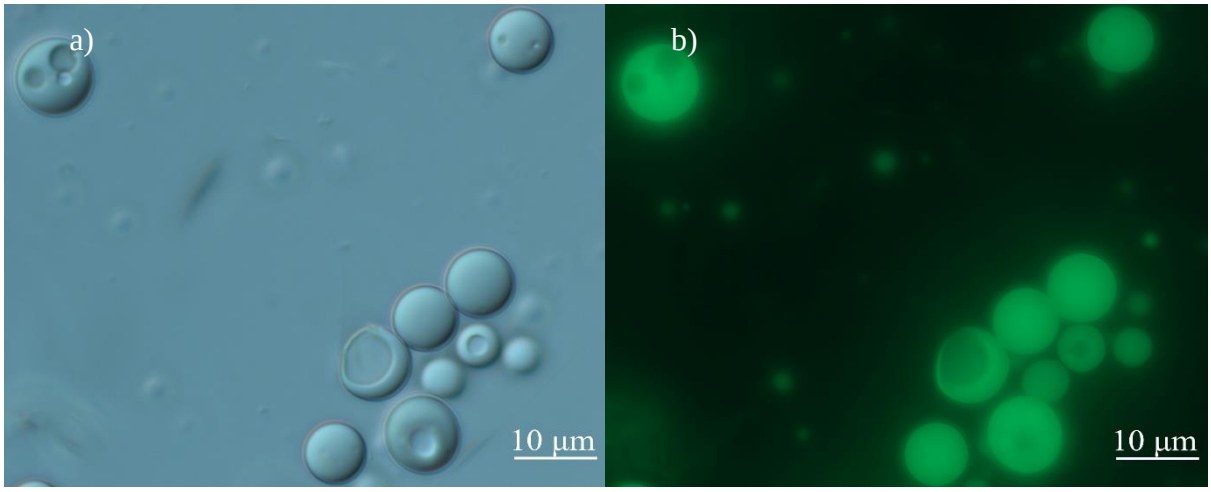

Figure 4.6 PLGA 50:50 (38,000-54,000 Da) spheres, visualized by a) DIC microscopy and b) fluorescence microscopy.

The unexpected core-shell morphology could be rationalized by considering the slow kinetics of high molecular weight polymers. Aqueous cores that occurred during emulsification got kinetically trapped as the high molecular weight polymers did not have time to equilibrate

during the solvent evaporation. This hypothesis could be tested by decreasing the evaporation rate of the volatile solvent during capsule formulation, but due to the limited time frame of the master's project this was not prioritized. However, it should be clarified, that microspheres of the high molecular weight grade of PLLA did not get a core-shell morphology. In this case, no aqueous cores were seen in the microscopy analysis during solvent evaporation either, so the probable reason for the more homogenous spherical geometry was the more hydrophobic nature of PLLA.

Another microscopy observation, that should be addressed, relates to the loading capacity of the microspheres. Recall that core-shell particle formulations containing 6 wt% tralopyril resulted in saturated capsules and fallen-out biocide that crystallized in suspension (Section 4.2). Saturated microspheres behaved identically. Polarized images of two batches of PLGA 70:30 spheres, loaded with different amounts of tralopyril, are presented in Figure 4.7. Note that the amount of crystalline tralopyril in suspension was significantly higher when loaded with 10 wt% (Figure 4.7a), compared to when loaded with 5 wt% (Figure 4.7b). This indicated a maximum solubility in the polymer closer to 5 wt%. All microsphere formulations tested throughout the project became saturated when loaded with 10 wt% tralopyril. Actual loading capacities were determined in the release studies (Section 4.3.3).

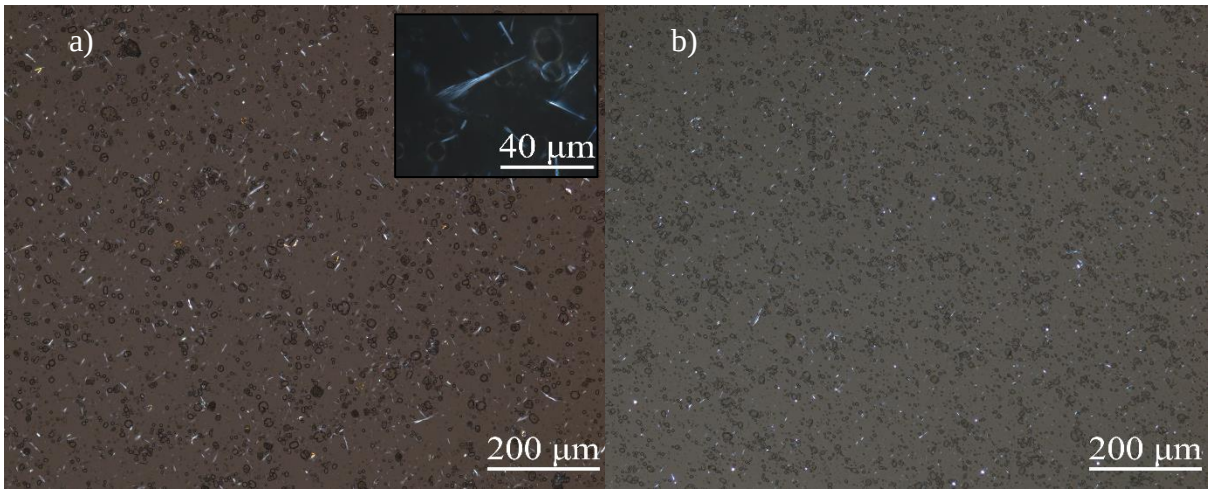

Figure 4.7 Polarized light microscopy of PLGA 70:30 sphere suspensions, in which needles of crystallized tralopyril can be seen. The biocide loadings were a) 10 wt% tralopyril and b) 5 wt % tralopyril. Note that the amount of crystalline material decreases with the tralopyril content. The inset to the top right in a) shows the crystals in a higher magnification.

Polarized light microscopy confirmed that formulations with semi-crystalline polymers (PLLA and P3(HB)) gave semi-crystalline microspheres. PLLA spheres are shown in Figure 4.8.

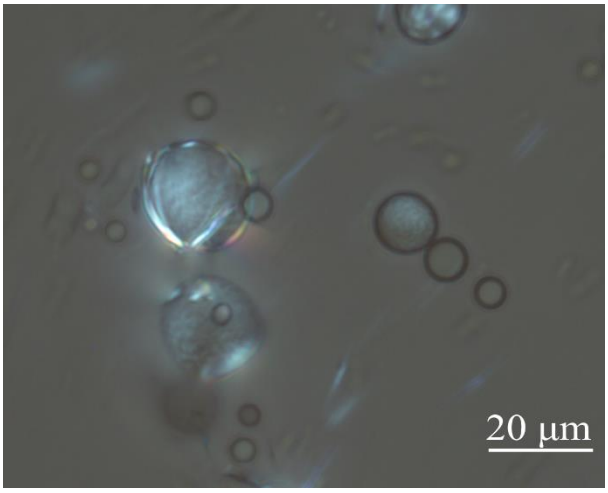

Figure 4.8 PLLA microspheres visualized by polarized light microscopy.

The P3(HB) spheres need to be further discussed as the PHA type of polymer resulted in fragmented and broken microcapsules, only a few particles of a spherical geometry could be observed (Figure 4.9a). Studied in polarized light (Figure 4.9b) the semi-crystalline nature of the polymeric fragments was visualized. There are two plausible explanations for the broken capsules, both relating to the chemical and physical properties of the polymer. First, it could be an effect of the exceptional stereoregularity and high degree of crystallinity, making P3(HB) a stiff, but also brittle material. The magnetic stirring during solvent evaporation might have been sufficiently forceful to damage the brittle polymeric spheres. Second, another option is that the low glass transition temperature (5 °C) gave the polymer a too high mobility to stay in the spherical conformation during the solvent evaporation.

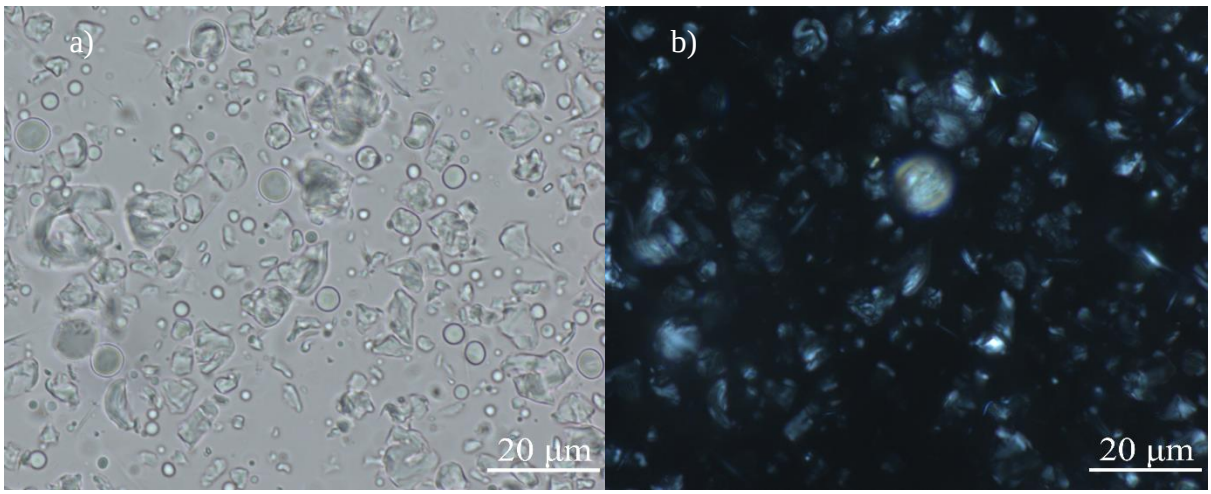

Figure 4.9 P3(HB) spheres, visualized by a) brightfield microscopy and b) polarized light microscopy.

4.3.2 Size distributions

Microsphere size distributions are summarized through the mean radii, μ_r, and standard deviations, σ_r, and presented in Table 4.2. Note that the parameters are calculated for microsphere formulations loaded with 10 wt% tralopyril, as this ensured that the results were comparable since all polymers got saturated below that concentration. However, a lower biocide loading barely affected the size distribution. For example, PLGA 70:30 spheres loaded with 5 wt% tralopyril had a mean radius of 1.82 µm, which is very close to the mean radius of the PLGA 70:30 spheres loaded with 10 wt% tralopyril (Table 4.2, label E, μ_r = 1.87 µm). At least 500 particles were counted and analyzed for each batch to obtain results with high certainty, except for the PLGA 70:30 batches (~100 particles) due to an insufficient number of microscopy images. It was not possible to determine the size distribution of the P3(HB) spheres because of their heavily fragmented nature.

Table 4.2 Mean radii (μ_r) and standard deviations (σ_r) for microspheres formulated with the different polymers used throughout the project. The specified values represent sphere batches loaded with 10 wt% tralopyril.

Label	μ_r (µm)	σ_r (µm)
A	1.85 ± 0.11	1.08 ± 0.52
B	2.08 ± 0.12	1.17 ± 0.54
C	1.92 ± 0.13	1.31 ± 0.63
D	1.42 ± 0.07	0.73 ± 0.33
E	1.87 ± 0.29	1.15 ± 0.80
F	1.92 ± 0.12	1.16 ± 0.56
G	1.94 ± 0.12	1.15 ± 0.54

Nevertheless, the similar values μ_r and σ_r for different sphere batches indicated a high reproducibility in the formulation process. Note that the sizes of the high molecular weight grades of PLGA (Table 4.2, label C and D) are not larger than the other microspheres. While it was difficult to quantify the amount of encapsulated water by visual inspection of the microscopy images, the results from the size determination suggests that the amount is negligible. This is positive since it makes the diffusion model for homogenous spheres (Equation 2.10) applicable. A typical size distribution is shown in Figure 4.10.

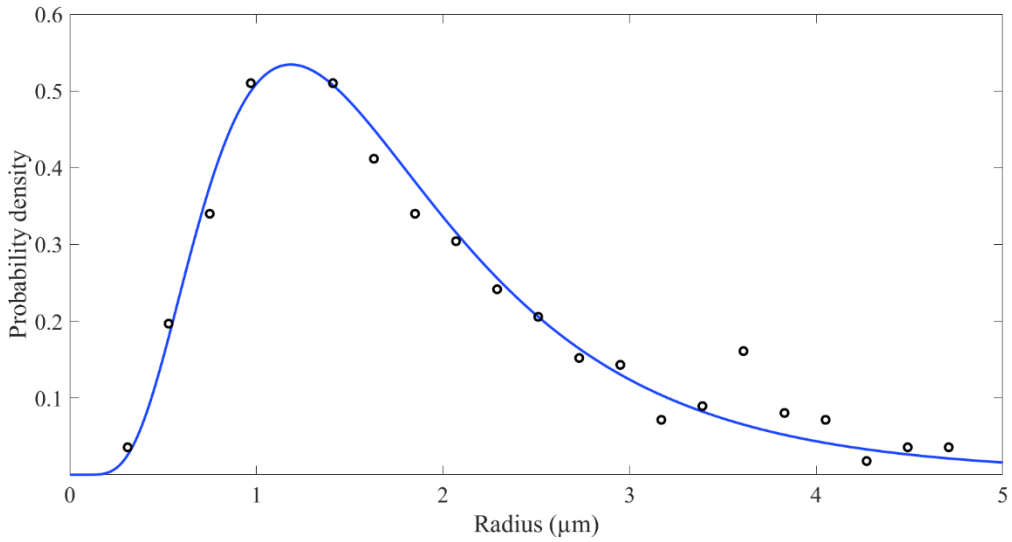

Figure 4.10 Size distribution of PLGA 50:50 (ester terminated) spheres, with the experimentally determined data points fitted to a log-normal distribution function (solid line).

4.3.3 Release studies of microsphere suspensions

From the release studies it was possible to calculate the loading capacities, *LC*, and the apparent diffusion coefficients, *D*, for the different microsphere batches. The results are summarized and presented in Table 4.3. Note that it was not possible to determine apparent diffusion coefficients for all sphere batches. For some batches (Table 4.3, label C, D and G) this was because the release was sustained significantly, so that the measurements were not close to completion at the end date of the master's project. Fitting a model to the experimental data would then give very arbitrary results with no real physical interpretation. Also be aware that the only completed studies concerned the release from PLGA 70:30 spheres (Table 4.3, label E), so that the fitted diffusion coefficients for other batches might deviate slightly from their true value. Another case, where the diffusion coefficient could not be estimated, was the P3(HB) batch (Table 4.3, label H), due to the broken and irregular geometry of the microparticles. Calculated loading capacities have an estimated uncertainty of 0.5 percentage points.

Table 4.3 Loading capacity (*LC*) and apparent diffusion coefficients (*D*) for microspheres formulated with the different polymers used throughout the project. The calculated loading capacities have an estimated uncertainty of 0.5 percentage points. The specified values represent sphere batches loaded with 10 wt% tralopyril.

Label	*LC* (wt%)	$D \cdot 10^{20}$ (m^2/s)
A	5.0	3.59
B	4.3	13.0
C	3.9	-
D	4.7	-
E	4.9	20.5
F	7.1	0.619
G	3.8	-
H	3.0	-

Before analyzing individual results, a short overall discussion about the effect of each screened parameter (chemical composition, molecular weight, degree of crystallinity and type of end-group of the polymer) is warranted. The chemical composition made a large difference, especially for low molecular weight polymer grades. Lactic-based polymers (PLA, PLLA and PLGA) had higher loading capacities and more sustained release profiles compared to P3(HB). However, this was certainly a consequence of the poor encapsulation outcome for the P3(HB) spheres. Moreover, out of the lactic-based polymers, the best performing by far was PLA (Table 4.3, label F). PLA had a significantly higher loading capacity (7.1 wt%) and a significantly more sustained release ($D = 0.619 \cdot 10^{-20}$ m^2/s) in comparison with the others.

Moving on, the molecular weight also made an impact. Regarding the loading capacity it was difficult to draw any conclusion. A higher molecular weight grade might decrease the encapsulation efficiency as both the high molecular weight grades of PLGA 50:50 and PLLA had calculated loading capacities below 4 wt% (Table 4.3, label C and G). However, the high molecular weight grade of PLGA 65:35 (Table 4.3, label D) contradicts this relation with a loading capacity of 4.7 wt%. What certainly could be concluded though, was that a higher molecular weight led to a more sustained release. Neither of the high molecular weight polymer sphere batches released enough tralopyril for diffusion models to be fitted, during the whole course of the master's project.

Lastly, the effects of the crystallinity and end-group of the polymers need to be addressed. It was difficult to draw any conclusions concerning the crystallinity, since the semi-crystalline polymers (PLLA and P3(HB)) were so chemically different otherwise. PLLA showed a very

sustained release, but it was not possible to deduce if this was an effect of the chemical composition, the molecular weight or the crystallinity. As for the end-group of the polymer, it could be concluded that it neither affected the loading capacity nor the release rate significantly. Both ester- and acid-terminated PLGA 50:50 (Table 4.3, label A and B) had similar loading capacities and diffusion coefficients.

4.3.3.1 Release profiles for different batches

In order to properly understand the release profile for a saturated microsphere formulation, it is appropriate to first study the release from batches with varying biocide loadings. The fractional release from PLGA 70:30 microspheres loaded with either 10 wt% or 5 wt% tralopyril is shown in Figure 4.11. Note the logarithmic x-axis.

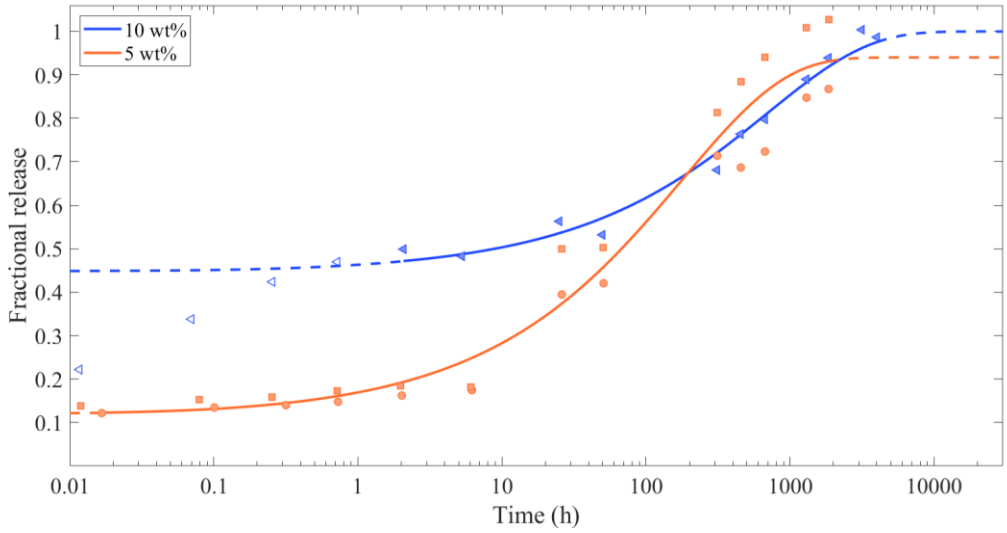

Figure 4.11 Fractional release from PLGA 70:30 microspheres loaded with either 10 wt% or 5 wt% tralopyril. The orange squares and circles, respectively, represent two replicate release studies for the 5 wt% batch. Filled marker symbols indicate that the release models have been fitted according to the experimental data, whereas unfilled marker symbols indicate that the experimental data has been excluded from the fit. Similarly, solid lines indicate that the model fitting is within the range of the fitted experimental data, and dashed lines indicate that the model is outside that range. Note the logarithmic x-axis.

Recall that already from the microscopy characterization (Section 4.3.1), it became clear that the saturation concentration in the PLGA 70:30 was close to 5 wt% because of the large amount of fallen-out and crystalline tralopyril in suspension for the 10 wt% loading. This can also be understood from the release profiles of the different batches. For a loading of 5 wt%, any crystalline tralopyril in suspension is rapidly dissolved (<0.01 h ≈ 0.5 min), and the increase in biocide concentration in the aqueous phase is thereafter slow and diffusion-controlled. Another behavior is observed for the 10 wt% loading where a relatively sharp increase in tralopyril concentration occurs during the first hour (indicated by blue unfilled markers in Figure 4.11). This increase is to a large extent caused by dissolution of crystalline tralopyril in suspension, rather than diffusional leakage from the microspheres, which is why those experimental data points has been excluded from the fitting of the diffusion model. Diffusion from microsphere suspensions is modelled through Equation 2.13.

Loading capacities can be calculated from the amount of tralopyril that did not fall out and crystallize in suspension. For example, for the 5 wt% loaded batch approximately 15% of the tralopyril content was not encapsulated, giving it a loading capacity of 4.5 wt%

(0.85 · 5 wt%). For the 10 wt% batch the loading capacity was determined to be 4.9 wt%. Note that the capacities of the two different batches lie within the estimated uncertainty of 0.5 percentage points.

Apart from the amount of crystalline tralopyril in suspension the release profiles of the PLGA 70:30 batches are very similar, as expected. Fitted diffusion coefficients are of the same orders of magnitude, $69.8 \cdot 10^{-20}$ m^2/s and $20.5 \cdot 10^{-20}$ m^2/s for the 5 wt% and 10 wt% loadings, respectively. The lower estimate for the 10 wt% batch might be attributed to the narrower data range, for which the fitting was made, due to removed data points associated with dissolution of crystalline tralopyril.

With the crystalline dissolution in mind, interpretation of the coming release profiles will be more straightforward. In Figure 4.12 the release profiles for sphere batches of three low molecular weight lactic-based polymers (PLGA 50:50, PLGA 70:30 and PLA) are shown. The difference between the polymers is an increased amount of LA, from 50% to pure PLA. The PLGA 50:50 batch did not display a remarkable loading capacity, even though that would be assumed by noting the biocide fraction left after dissolution of crystals, as the PLGA 50:50 formulation was actually loaded with slightly less than 10 wt% tralopyril. Loading capacities were 4.3 wt%, 4.9 wt% and 7.1 wt% for PLGA 50:50, PLGA 70:30 and PLA, respectively. The apparent diffusion coefficients were determined to be $13.0 \cdot 10^{-20}$ m^2/s, $20.5 \cdot 10^{-20}$ m^2/s and $0.619 \cdot 10^{-20}$ m^2/s, respectively.

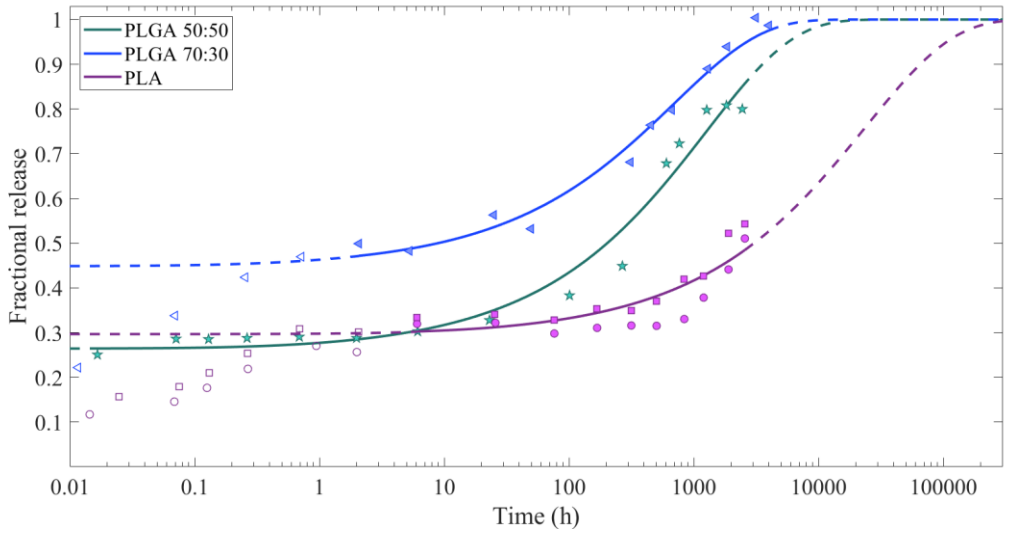

Figure 4.12 Fractional release from low molecular weight grades of PLGA 50:50, PLGA 70:30 and PLA microspheres, respectively, loaded with 10 wt% tralopyril. The purple squares and circles represent two replicate release studies for the PLA batch. Filled marker symbols indicate that the release models have been fitted according to the experimental data, whereas unfilled marker symbols indicate that the experimental data has been excluded from the fit. Similarly, solid lines indicate that the model fitting is within the range of the fitted experimental data, and dashed lines indicate that the model is outside that range. Note the logarithmic x-axis.

Since the different PLGA grades have very similar loading capacities and release profiles, it can be concluded that varying the LA:GA ratio within this range does not affect the outcome. The slight difference in release characteristics can be attributed to the uncertainty in the experimentally collected data. Multiple factors can affect the release, including a slight temperature variation on different magnetic stirrers in the laboratory. On the other hand, PLA

had a significantly higher loading capacity and considerably slower release. Note that almost all tralopyril from the PLGA spheres had been released after circa 4,000 h, which is approximately a half-year. The PLA spheres are predicted by the diffusion model to have released the same fraction after circa 200,000 h, which is more than 20 years. It is important to know that the release measurements are designed so that the apparent diffusion coefficient can be estimated and that the actual release time is less important. When the diffusion coefficient is determined the release time can be modified by changing the sizes of the spheres, smaller spheres have a faster release.

The superior performance of the PLA spheres was the reason they were chosen to be incorporated in a marine paint system (Section 4.4). Why the PLA spheres were especially suited for encapsulation of tralopyril might have to do with the relatively high hydrophobicity of the polymer, providing a favorable environment for the aromatic structures of the biocide.

In Figure 4.12 the release profiles for sphere batches of three high molecular weight lactic-based polymers (PLGA 50:50, PLGA 65:35 and PLLA) are presented. The PLGA grades are amorphous, while PLLA is semi-crystalline. Because neither of the release studies are close to completion no diffusional model has been fitted to the experimental data, which is also a reason why it is yet not possible to see any trends in their apparent diffusion coefficients. What can be observed though, is that the release for high molecular weight polymer grades is slower and more sustained compared to low molecular weight grades. This is likely caused by a less efficient polymer packing and a higher tortuosity. It is also reasonable to assume that the semi-crystalline properties of PLLA further sustained the release by decreasing the permeability of the biocide through the capsule matrix. However, because so many other factors are different for PLLA compared to the other tested polymers, it was not possible to deduce if this was an effect of the chemical composition, the molecular weight or the crystallinity.

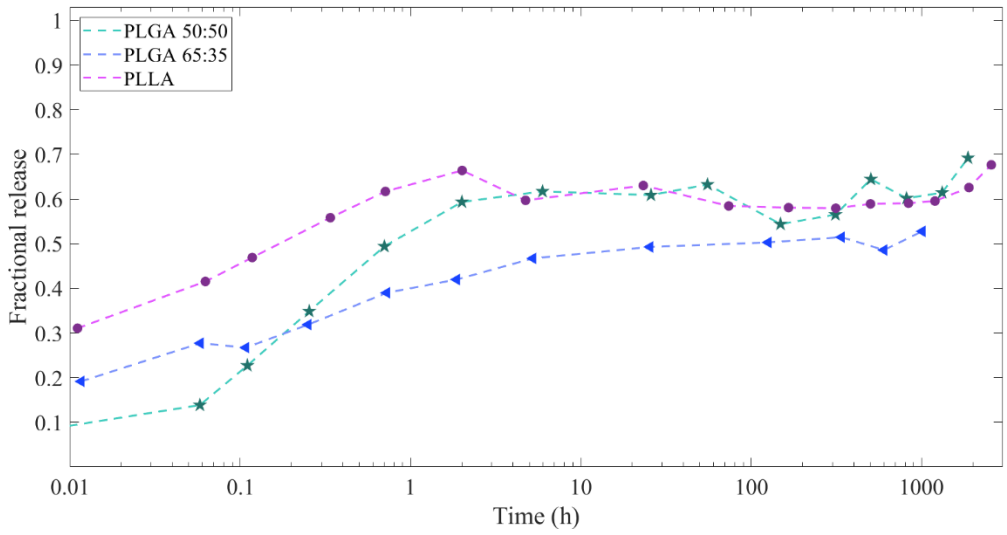

Figure 4.13 Fractional release from high molecular weight grades of PLGA 50:50, PLGA 65:35 and PLLA microspheres, respectively, loaded with 10 wt% tralopyril. Because neither of the release studies are close to completion no diffusional model has been fitted to the experimental data. Note the logarithmic x-axis.

For a complete discussion on how the chemical composition affects the encapsulation efficiency and release properties, the fractional release from the P3(HB) spheres is shown in Figure 4.14. Because of the broken and highly fragmented nature of the capsules no diffusional model has been fitted to the experimental data. Note that the encapsulation efficiency is very poor, fallen-out and crystallized tralopyril accounts for 70% of the total amount. This gives P3(HB) a loading capacity of circa 3.0 wt%.

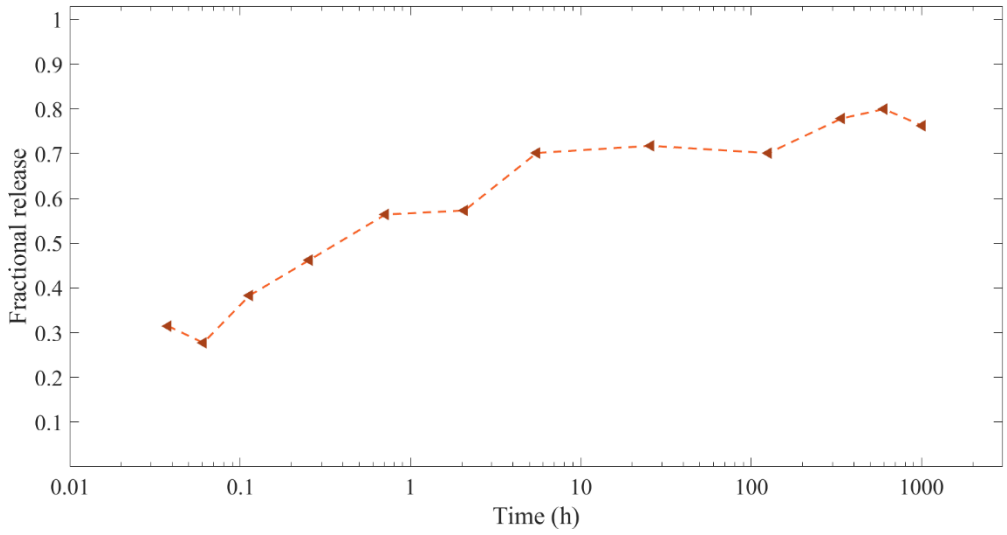

Figure 4.14 Fractional release from P3(HB) microspheres loaded with 10 wt% tralopyril. Because of the broken and highly fragmented nature of the capsules no diffusional model has been fitted to the experimental data. Note the logarithmic x-axis.

Lastly, the effect of the end-group is clarified by Figure 4.15, which shows the release from two low molecular weight grades of PLGA 50:50, either ester- or acid-terminated.

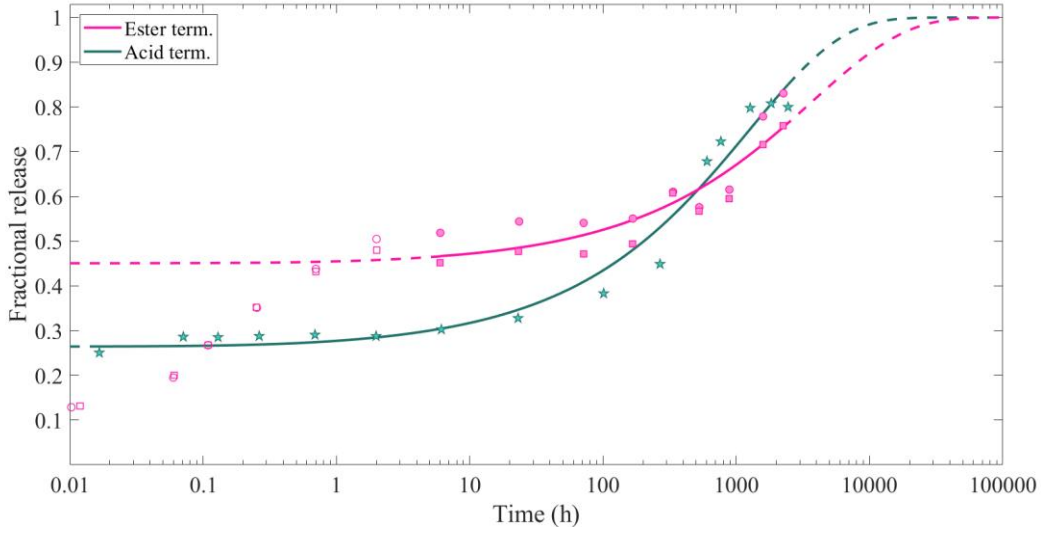

Figure 4.15 Fractional release from microspheres of two low molecular weight grades of PLGA 50:50, either ester- or acid-terminated, loaded with 10 wt% tralopyril. The pink squares and circles represent two replicate release studies for the ester-terminated batch. Filled marker symbols indicate that the release models have been fitted according to the experimental data, whereas unfilled marker symbols indicate that the experimental data has been excluded from the fit. Similarly, solid lines indicate that the model fitting is within the range of the fitted experimental data, and dashed lines indicate that the model is outside that range. Note the logarithmic x-axis.

In Figure 4.15 the ester-terminated batch appears to contain a larger fraction of crystalline tralopyril in suspension compared to the acid-terminated batch, but in this case, this is not attributed to a lower loading capacity. Recall that the acid-terminated PLGA 50:50 batch was loaded with a little less than 10 wt% tralopyril, causing the remaining fraction in the capsules after crystalline dissolution to be larger compared to the ester-terminated batch, even though their loading capacities are similar. Loading capacities are 5.0 wt% and 4.3 wt%, for the ester-terminated and acid-terminated batch, respectively. Diffusion coefficients are within the same order of magnitude, $3.59 \cdot 10^{-20}$ m^2/s and $13.0 \cdot 10^{-20}$ m^2/s, respectively. Because of the similar loading capacities and release profiles for the two low molecular weight PLGA 50:50 batches, the effect of the end-group of the polymer could be concluded to be negligible. This is expected since the end-groups contribution to the overall chemical composition of the polymer is very low. If the end-group had interacted through bonding with the biocide it would have made a larger impact, however, so is evidently not the case.

4.4 Antifouling coatings

Recall from Section 3.5 that three different paint formulations were used to coat plates. Those were (i) unmodified, biocide-free, paint from Steen-Hansen, (ii) reformulated paint containing molecularly free biocide, and (iii) reformulated paint containing encapsulated biocide. After the plates had been coated, a microscopy analysis was carried out to determine if the free biocides and the microspheres, respectively, had been dispersed successfully, see Figure 4.16.

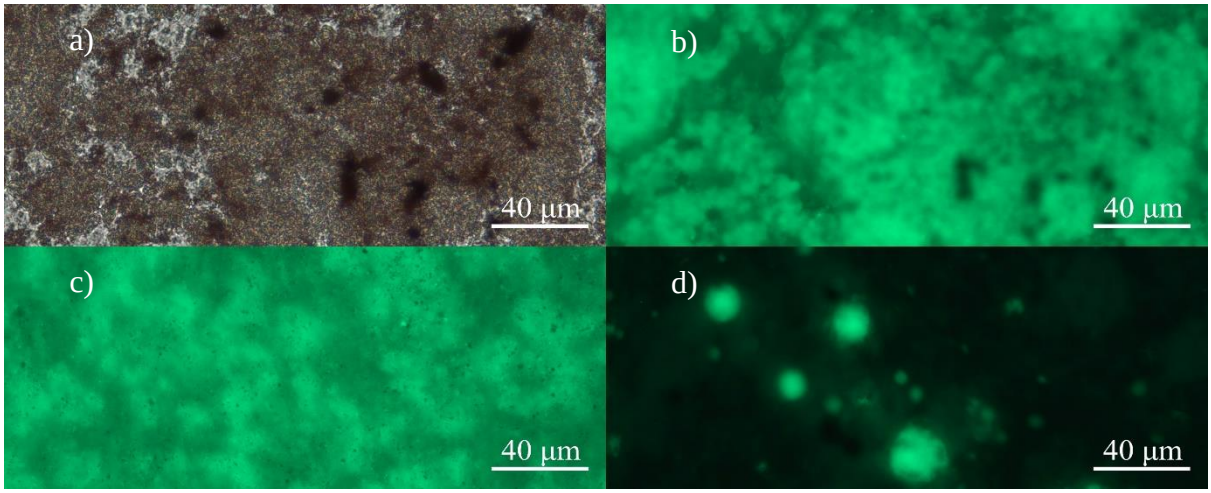

Figure 4.16 Microscopy images of the marine coatings. The top row shows unmodified, biocide-free, paint from Steen-Hansen in a) a brightfield micrograph, and b) a fluorescence micrograph. The bottom row displays fluorescence micrographs of reformulated Steen-Hansen paint, either containing c) molecularly free biocide, or d) encapsulated biocide.

Note that the binder material in Steen-Hansen's (biocide-free) paint fluoresced (Figure 4.16b) in the same wavelength range as tralopyril, making it more difficult to locate the molecularly free biocide in the reformulated paint (Figure 4.16c). Still, the fluorescence from the reformulated paint, with molecularly free biocide, appeared homogenous as no biocide aggregates with a more intense fluorescence could be seen. It was therefore assumed that the biocide was well dispersed. In the reformulated paint containing encapsulated tralopyril (Figure 4.16d), intact and well dispersed microspheres were identified by fluorescence microscopy. The paint reformulation had hence been successful.

Recall (Section 3.5) that plates were coated with a 100 µm thick layer paint. After drying, the coating thickness was determined through a profilometry analysis to be 27 ± 10 µm (mean ± sample standard deviation). This was well in line with the weight loss as the coatings dried. Dry coatings weighed 20 ± 12 wt% of the wet coatings weight. The coating thickness (L) is a parameter needed to model diffusion in a plane sheet (Section 2.7.2).

4.4.1 Release studies of antifouling coatings

The release from coatings with molecularly free biocide have been compared to the release from coatings containing encapsulated biocide, see Figure 4.17. The released amount has been quantified from tralopyril and its degradation product. Note that after approximately 300 h the release measurements were far from completion since less than 7% of the total amount of tralopyril had been released. No diffusional model has hence been fitted to the experimental data.

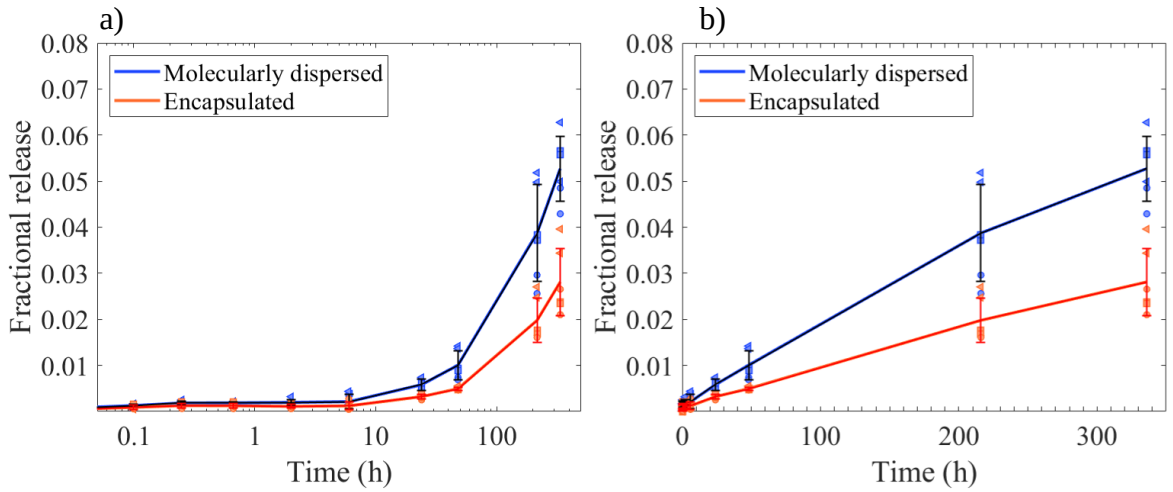

Figure 4.17 Release from coatings presented on a) a logarithmic time scale and b) a linear scale. The release from coatings with molecularly free biocide is compared to the release from coating with encapsulated biocide. Different marker symbols (triangles, circles and squares) indicate different release bath, 3 replicate release bath was studied for each coating formulation. The standard deviation of the released amount is indicated with error bars.

The release was very slow for both the freely dispersed tralopyril and the encapsulated tralopyril. Comparing with the release measurements for the microsphere suspensions, most sphere formulations with a low molecular weight polymer (the exception being PLA) had released a considerably larger fraction after 300 h than the coatings. The release behavior from the coatings seems to be more reminiscent of the release behavior of high molecular sphere formulations. The binder material might provide a matrix of similar tortuosity as the high molecular weight sphere matrices, which would explain the resemblance in release profiles.

For the freely dispersed tralopyril the effective diffusion was only dependent on the pore-structure of the coating binder matrix (9), whereas for the encapsulated tralopyril the effective diffusion was affected by two separate elements; (i) diffusion through the microspheres followed by (ii) a diffusion through the binder matrix. While it is yet too early to fit any diffusion models to the experimental data, it should still be noted that the microspheres

significantly decrease the biocidal release rate from the coating. In the latest samples taken, twice as much tralopyril has been released from the coatings with freely dispersed biocide. As the measurements progress the relative difference will increase further.

Lastly, a slight concern that needs to be addressed, has to do with the blank artificial seawater samples that were spiked with tralopyril, as a means to follow the hydrolysis of tralopyril during storage. All spiked reference samples had lost over 90 wt% of their original tralopyril content at the time of the LC-MS/MS measurements. Also, no degradation product was detected in them, indicating that this was due to some source of error rather than hydrolysis of tralopyril. This has not been accounted for in the experimental data presented in Figure 4.17, since it was impossible to know if loss had occurred in those samples as well and to which extent.

5
Conclusion

A controlled and sustained biocidal release is desired for a long-term antifouling protection by marine coatings. This can be achieved through microencapsulation of the biocides. In this project several microcapsule systems have been screened and assessed based on their loading capacities and release characteristics. Further, the most promising capsules have been incorporated in a marine paint system, where their performance has been evaluated relative to commercial paint with freely dispersed biocide. When apparent diffusion coefficients have been determined, the diffusion-dependent release can be tuned by modifying the size of the microcapsules.

Two different microcapsule morphologies have been evaluated, core-shell particles and monolithic microspheres, respectively. A successful encapsulation in core-shell particles would have many benefits as the shell material's barrier properties hinder immediate release, while at the same time protecting the active. However, due to a preferential but disadvantageous partitioning of tralopyril in the shell compared to the core of the capsules, the core-shell morphology could be discarded as it had no advantages over the homogenous microspheres.

Polymeric matrix materials, for the microspheres, were screened based on chemical composition, molecular weight, degree of crystallinity and type of end-group. Different aliphatic polyesters were tested, ranging from PHB to lactic-based polymers (PLA, PLLA and PLGA). The chemical composition made a big impact. When formulating with P3(HB) the outcome was heavily fragmented and broken microspheres, probably caused by the brittleness of the highly crystalline polymer. P3(HB) microparticles had a poor encapsulation efficiency of 3.0 wt%. On the other hand were the lactic-based polymers performing significantly better, with loading capacities around 5 wt% and sustained release characteristics ($D = 20.5 \cdot 10^{-20}$ m^2/s for PLGA 70:30). Varying the LA:GA ratio within a range of 50-70% LA content made little difference, but a large effect could be seen when switching to pure PLA. PLA had a superior loading capacity (7.1 wt%) and a considerably slower release ($D = 0.619 \cdot 10^{-20}$ m^2/s) in comparison with the others. A possible explanation why was that the relatively high hydrophobicity of PLA provided a favorable environment for the aromatic structures of the biocide.

Increasing the molecular weight also highly influenced the capsule characteristics. Because of this, the effect of chemical composition was observed less for high molecular weight grades. A higher molecular weight led to a more sustained release and potentially also a lower encapsulation efficiency, although more polymers need to be studied to confirm this.

Regarding the crystallinity, a higher crystallinity should be associated with a low permeability through the polymer matrix and thus a slower release. However, it was difficult to draw any experimental conclusions, since the investigated semi-crystalline polymers (PLLA and P3(HB)) were so chemically different otherwise. Lastly, the end-group of the polymer did not affect the loading capacity nor the release characteristics of the biocide.

Incorporation of PLA spheres in a marine paint was successful. The release from antifouling coatings was slow already for paint containing freely dispersed biocide, probably due to a high tortuosity of the binder matrix. However, when encapsulated the biocidal release rate was decreased significantly compared to the freely dispersed tralopyril. By tuning the molecular diffusion in microcapsules, a controlled and sustained biocidal release from antifouling coating can hence be achieved.

For future studies it is of interest to see if the prerequisites for a successful encapsulation of tralopyril, regarding capsule morphology and material choices, also applies to other biocides. For instance medetomidine, which is a biocide efficient against growth of microorganisms with a nervous system . Regarding the continuous work with tralopyril, the next step would be to conduct microbiology studies to evaluate the performance of the antifouling coatings in a real marine environment.

Bibliography

1. Jin H, Tian L, Bing W, Zhao J, Ren L. Toward the Application of Graphene for Combating Marine Biofouling. Advanced Sustainable Systems. 2021;5(1):2000076.

2. Sarkar PK, Pawar SS, Rath SK, Kandasubramanian B. Anti-barnacle biofouling coatings for the protection of marine vessels: synthesis and progress. Environ Sci Pollut Res. 2022 Jan 25;1–35.

3. Bixler GD, Bhushan B. Biofouling: lessons from nature. Phil Trans R Soc A. 2012 May 28;370(1967):2381–417.

4. Yebra DM, Kiil S, Dam-Johansen K. Antifouling technology—past, present and future steps towards efficient and environmentally friendly antifouling coatings. Progress in Organic Coatings. 2004 Jul;50(2):75–104.

5. Wehrspohn RB, Hirsch U. Prevention of Biofouling. In: Neugebauer R, editor. Biological Transformation. Berlin, Heidelberg: Springer; 2020. p. 329–49.

6. Jones G. 2 - The battle against marine biofouling: a historical review. In: Hellio C, Yebra D, editors. Advances in Marine Antifouling Coatings and Technologies. Woodhead Publishing; 2009. p. 19–45. (Woodhead Publishing Series in Metals and Surface Engineering).

7. Koning JT, Bollmann UE, Bester K. Biodegradation of third-generation organic antifouling biocides and their hydrolysis products in marine model systems. Journal of Hazardous Materials. 2021 Mar;406:124755.

8. Andersson Trojer M, Nordstierna L, Bergek J, Blanck H, Holmberg K, Nydén M. Use of microcapsules as controlled release devices for coatings. Advances in Colloid and Interface Science. 2015 Aug;222:18–43.

9. Bergek J, Andersson Trojer M, Mok A, Nordstierna L. Controlled release of microencapsulated 2-n-octyl-4-isothiazolin-3-one from coatings: Effect of microscopic and macroscopic pores. Colloids and Surfaces A: Physicochemical and Engineering Aspects. 2014 Sep;458:155–67.

10. Ciriminna R, Bright FV, Pagliaro M. Ecofriendly Antifouling Marine Coatings. ACS Sustainable Chem Eng. 2015 Apr 6;3(4):559–65.

11. Gullberg E, Cao S, Berg OG, Ilbäck C, Sandegren L, Hughes D, et al. Selection of Resistant Bacteria at Very Low Antibiotic Concentrations. PLOS Pathogens. 2011 Jul 21;7(7):e1002158.

12. Andersson Trojer M, Nordstierna L, Nordin M, Nydén M, Holmberg K. Encapsulation of actives for sustained release. Phys Chem Chem Phys. 2013;15(41):17727.

13. Eriksson V. Sustained and triggered release by microencapsulation [Licentiate thesis]. [Gothenburg]: Chalmers University of Technology; 2021.

14. Dubey R, Shami TC, Rao KUB. Microencapsulation Technology and Applications. DEF SCI J. 2009;59(1):14.

15. Loxley A, Vincent B. Preparation of Poly(methylmethacrylate) Microcapsules with Liquid Cores. Journal of Colloid and Interface Science. 1998 Dec;208(1):49–62.

16. Andersson Trojer M, Li Y, Abrahamsson C, Mohamed A, Eastoe J, Holmberg K, et al. Charged microcapsules for controlled release of hydrophobic actives. Part I: encapsulation methodology and interfacial properties. Soft Matter. 2013;9(5):1468–77.

17. Eriksson V. Core-shell particles based on biopolymers and bioactive fatty acids. Encapsulation, characterization and release [Master's thesis]. [Gothenburg]: Chalmers University of Technology; 2019.

18. Rennie R, Law J, editors. glycerides (acylglycerols). In: Dictionary of chemistry. Eight edition. Oxford, United Kingdom ; New York, NY: Oxford University Press; 2020. (Oxford quick reference).

19. Ash M, Ash I. Ethyl linoleate. In: Handbook of Solvents. 3rd ed. Synapse Information Resources Inc.; 2018.

20. Salvatore MM, Alves A, Andolfi A. Secondary Metabolites Produced by Neofusicoccum Species Associated with Plants: A Review. Agriculture. 2021 Feb 11;11(2):149.

21. Jaraswekin S, Prakongpan S, Bodmeier R. Effect of poly(lactide-co-glycolide) molecular weight on the release of dexamethasone sodium phosphate from microparticles. Journal of Microencapsulation. 2007 Jan 1;24(2):117–28.

22. Izumikawa S, Yoshioka S, Aso Y, Takeda Y. Preparation of poly(l-lactide) microspheres of different crystalline morphology and effect of crystalline morphology on drug release rate. Journal of Controlled Release. 1991 Apr 1;15(2):133–40.

23. Yadav SK, Khilar KC, Suresh AK. Release rates from semi-crystalline polymer microcapsules formed by interfacial polycondensation. Journal of Membrane Science. 1997 Mar 19;125(2):213–8.

24. Eriksson V, Nygren E, Andersson Trojer M, Evenäs L. Encapsulation and Sustained Release of Octenidine Dihydrochloride from PLGA Microcapsules. [Unpublished manuscript]. 2022.

25. Davachi SM, Kaffashi B. Polylactic Acid in Medicine. Polymer-Plastics Technology and Engineering. 2015 Jun 23;54(9):944–67.

26. Murariu M, Dubois P. PLA composites: From production to properties. Advanced Drug Delivery Reviews. 2016 Dec 15;107:17–46.

27. Avérous L. Chapter 21 - Polylactic Acid: Synthesis, Properties and Applications. In: Belgacem MN, Gandini A, editors. Monomers, Polymers and Composites from Renewable Resources. Amsterdam: Elsevier; 2008. p. 433–50.

28. Martins C, Sousa F, Araújo F, Sarmento B. Functionalizing PLGA and PLGA Derivatives for Drug Delivery and Tissue Regeneration Applications. Advanced Healthcare Materials. 2018;7(1):1701035.

29. Gentile P, Chiono V, Carmagnola I, Hatton PV. An Overview of Poly(lactic-co-glycolic) Acid (PLGA)-Based Biomaterials for Bone Tissue Engineering. International Journal of Molecular Sciences. 2014 Mar;15(3):3640–59.

30. Makadia HK, Siegel SJ. Poly Lactic-co-Glycolic Acid (PLGA) as Biodegradable Controlled Drug Delivery Carrier. Polymers. 2011 Sep;3(3):1377–97.

31. McAdam B, Brennan Fournet M, McDonald P, Mojicevic M. Production of Polyhydroxybutyrate (PHB) and Factors Impacting Its Chemical and Mechanical Characteristics. Polymers. 2020 Dec;12(12):2908.

32. Yeo JCC, Muiruri JK, Thitsartarn W, Li Z, He C. Recent advances in the development of biodegradable PHB-based toughening materials: Approaches, advantages and applications. Materials Science and Engineering: C. 2018 Nov;92:1092–116.

33. Kavitha G, Rengasamy R, Inbakandan D. Polyhydroxybutyrate production from marine source and its application. International Journal of Biological Macromolecules. 2018 May 1;111:102–8.

34. Dawes EA. Polyhydroxybutyrate: An intriguing biopolymer. Biosci Rep. 1988 Dec 1;8(6):537–47.

35. European Union. Regulation (EU) No 528/2012 of the European Parliament and of the Council of 22 May 2012 concerning the making available on the market and use of biocidal products. Off J Eur Union L. 2012;167.

36. Kibenge FSB, Baldisserotto B, Chong RSM, editors. Aquaculture toxicology. 1st ed. Waltham: Elsevier; 2020.

37. Chen X, Zheng J, Teng M, Zhang J, Qian L, Duan M, et al. Tralopyril affects locomotor activity of zebrafish (Danio rerio) by impairing tail muscle tissue, the nervous system, and energy metabolism. Chemosphere. 2022 Jan;286:131866.

38. Yebra D, Weinell C. Key issues in the formulation of marine antifouling paints. In: Advances in Marine Antifouling Coatings and Technologies. Elsevier; 2009. p. 308–33.

39. Zuin S, Massari A, Ferrari A, Golanski L. Formulation effects on the release of silica dioxide nanoparticles from paint debris to water. Science of The Total Environment. 2014 Apr 1;476–477:298–307.

40. Crank J. The mathematics of diffusion. 2. ed., reprint. Oxford: Clarendon Press; 1976.

41. Günther H. NMR spectroscopy: basic principles, concepts and applications in chemistry. 3rd ed. Weinheim: Wiley-VCH; 2013.

42. Hollas JM. Modern spectroscopy. 4th ed. Chichester ; Hoboken, NJ: J. Wiley; 2004.

43. Lakowicz JR. Principles of fluorescence spectroscopy. 3rd ed. New York: Springer; 2016.

44. Harris DC. Quantitative chemical analysis. 8th ed. New York: W.H. Freeman and Co; 2010.

45. Glish GL, Vachet RW. The basics of mass spectrometry in the twenty-first century. Nat Rev Drug Discov. 2003 Feb;2(2):140–50.

DEPARTMENT OF CHEMISTRY AND CHEMICAL ENGINEERING
CHALMERS UNIVERSITY OF TECHNOLOGY
Gothenburg, Sweden 2022
www.chalmers.se

CHALMERS
UNIVERSITY OF TECHNOLOGY